Final Report for Interchange NCC2-5149
Computational Modeling of Semiconductor Dynamics at Femtosecond Time Scales

IN-33
372540

Govind P. Agrawal

The Institute of Optics

University of Rochester

Rochester, NY 14627 Phone: 716-275-4846 E-mail: gpa@optics.rochester.edu

Peter M. Goorjian

NASA Ames Research Center

Moffett Field, CA 94035 Phone: 415-604-5547 E-mail: goorjian@nas.nasa.gov

Funds for the support of this study has been allocated by the NASA-Ames Research Center, Moffett Field, California, under Interchange No. NCC2-5149.

CASI

Research Accomplishments

The main objective of the Joint-Research Interchange NCC2-5149 was to develop computer codes for accurate simulation of femtosecond pulse propagation in semiconductor lasers and semiconductor amplifiers [1]. The code should take into account all relevant processes such as the interband and intraband carrier relaxation mechanisms and the many-body effects arising from the Coulomb interaction among charge carriers [2]. This objective was fully accomplished. We made use of a previously developed algorithm developed at NASA Ames [3]–[5]. The new algorithm was tested on several problems of practical importance. One such problem was related to the amplification of femtosecond optical pulses in semiconductors. These results were presented in several international conferences over a period of three years.

With the help of a postdoctoral fellow, we also investigated the origin of instabilities that can lead to the formation of femtosecond pulses in different kinds of lasers. We analyzed the occurrence of absolute instabilities in lasers that contain a dispersive host material with third-order nonlinearities. Starting from the Maxwell–Bloch equations, we derived general multimode equations to distinguish between convective and absolute instabilities. We find that both self-phase modulation and intensity-dependent absorption can dramatically affect the absolute stability of such lasers. In particular, the self-pulsing threshold (the so-called second laser threshold) can occur at few times the first laser threshold even in good-cavity lasers for which no self-pulsing occurs in the absence of intensity-dependent absorption. These results were presented in an international conference and published in the form of two papers.

REFERENCES

1. Agrawal, G. P., and Dutta, N. K., *Semiconductor Lasers*, 2nd Ed. (Van Nostrand Reinhold, New York, 1993).

Research Project

The Interchange No. NCC2-5149 deals with the emerging technology of photonic (or optoelectronic) integrated circuits (PICs or OEICs). In PICs, optical and electronic components are grown together on the same chip. To build such devices and subsystems, one needs to model the entire chip. PICs are useful for building components for integrated optical transmitters, integrated optical receivers, optical data storage systems, optical interconnects, and optical computers. For example, the current commercial rate for optical data transmission is 2.5 gigabits per second, whereas the use of shorter pulses to improve optical transmission rates would yield an increase of 400 to 1000 times. The improved optical data transmitters would be used in telecommunications networks and computer local-area networks. Also, these components can be applied to activities in space, such as satellite to satellite communications, when the data transmissions are made at optical frequencies.

The research project consisted of developing accurate computer modeling of electromagnetic wave propagation in semiconductors. Such modeling is necessary for the successful development of PICs. More specifically, these computer codes would enable the modeling of such devices, including their subsystems, such as semiconductor lasers and semiconductor amplifiers in which there is femtosecond pulse propagation. Presently, there are no computer codes that could provide this modeling. Current codes do not solve the full vector, nonlinear, Maxwell's equations, which are required for these short pulses and also current codes do not solve the semiconductor Bloch equations, which are required to accurately describe the material's interaction with femtosecond pulses. The research performed under NCC2-5149 solves the combined Maxwell's and Bloch's equations.

2. Chow, W. W., Koch, S. W., and Sargent III, M., *Semiconductor-Laser Physics* (Springer-Verlag, New York, 1994).

3. Goorjian, P. M. and Taflove, A.,"Direct Time Integration of Maxwell's Equations in Nonlinear Dispersive Media for Propagation of Femtosecond Electromagnetic Solitons," *Optics Letters*, Vol. 17, No. 3, Feb. 1, 1992.

4. Goorjian, P. M., Taflove, A., Joseph, R. M., and Hagness, S. C., "Computational Modeling of Femtosecond Optical Solitons from Maxwell's Equations," *IEEE Journal of Quantum Electronics*, special issue on "Ultrafast Optics and Electronics," vol. 28, No. 10, pp. 2416-2422, Oct., 1992.

5. Goorjian, P. M., and Silberberg, Y., "Numerical Simulations of Light Bullets, Using the Full Vector, Time Dependent, Nonlinear Maxwell Equations." Integrated Photonics Research Topical Meeting, (IPR'95), February 23-25, 1995, at Dana Point, CA., cosponsored by Optical Society of America and IEEE/Lasers and Electro-Optics Society.

Publications

The results obtained during this research were presented in several international conferences and published in the form of two papers. The support of NASA-Ames was acknowledged in all publications. A list of publications follows. Copies of several publications are enclosed with this final report.

1. P. M. Goorjian and G. P. Agrawal, "Computational Modeling of ultrashort optical pulse propagation in nonlinear optical materials," Nonlinear Optics Conference, Maui, Hawaii, July 8-12, 1996.

2. G. H. M. van Tartwijk and G. P. Agrawal, "Generalized Lorenz-Haken dynamics and semiconductor lasers," paper WK5, Annual Meeting of the Optical Society of America, Rochester, NY, Oct. 20–25, 1996.
3. G. H. M. van Tartwijk and G. P. Agrawal, "Convective and absolute instabilities in fiber lasers ," Paper TuNN5, Annual Meeting of the Optical Society of America, Long Beach, CA, Oct. 12–17, 1997.
4. P. M. Goorjian and G. P. Agrawal, "Maxwell-Bloch Equations Modeling of Ultrashort Optical Pulse Propagation in Semiconductor Materials," Paper WB2, Annual Meeting of the Optical Society of America, Long Beach, CA, Oct. 12–17, 1997.
5. G. H. M. van Tartwijk and G. P. Agrawal, "Maxwell-Bloch dynamics of Modulation instabilities in fiber lasers and amplifiers," *J. Opt. Soc. Am. B***14**, 2618–2627 (1997).
6. G. H. M. van Tartwijk and G. P. Agrawal, "Absolute instabilities in lasers with host-induced dispersion and nonlinearities," *IEEE J. Quantum Electron.* **34**, October (1998).

Conf. on Nonlinear Optics, Hawaii, July 199

Computational Modeling of Ultrashort Pulse Propagation in Semiconductor Materials

Peter M. Goorjian
NASA Ames Research Center, M.S. T27B-1, Moffett Field, CA 94035-1000
Phone: (415) 604-5547, Fax: (415) 604-1095, Email: goorjian@nas.nasa.gov
Govind P. Agrawal
Institute of Optics, University of Rochester, Rochester, NY 14627
Phone: (716) 275-4846, Fax: (716) 244-4936, Email: gpa@optics.rochester.edu

An algorithm has been developed that solves the semiconductor Maxwell-Bloch equations [1], without making the standard approximations of a slowly-varying envelope (SVEA) and a rotating-wave (RWA). This more exact formulation is applied to simulations of the propagation of ultrashort pulses for which the standard approximations reach their limits. This development was motivated by the generation of optical pulses as short as 8 fs, which has become possible due to recent progress in ultrafast technology.

Previously, an algorithm was developed for the Maxwell equations [2,3], without making the SVEA for calculations of pulse propagation in nonlinear glasses, which exhibit Kerr-like instantaneous nonlinearities. It was found that significant differences can occur when the SVEA is not made in Maxwell equations. Specifically, light bullets, of 25 fs duration, were found to be stable [4] with the full Maxwell equations, whereas previously, calculations with the nonlinear Schroedinger equation had shown them to be unstable [5]. More recently [6], using the algorithm developed in references 2 and 3, calculations showed the formation of shock waves on the optical carrier wave. Such results are impossible with the SVEA since the carrier wave is eliminated from the calculations.

In this paper, this new algorithm is applied to studies of ultrafast optical pulse propagation in nonlinear semiconductor materials, in which many-body effects due to Coulomb interactions are included. In addition to the algorithm for Maxwell's equations, a new algorithm has been developed for the semiconductor Bloch equations that does not make the RWA and the two algorithms have been combined into one for the coupled semiconductor Maxwell-Bloch equations. In the Bloch equations the relaxation-time approximation [1] has been made for the various intraband scattering processes.

The Maxwell-Bloch equations for pulse propagation in one spatial dimension are the following. Assume that the electric field of a pulse that is propagating along the z direction is polarized along the x axis and ignore the transverse effects, then the Maxwell equations become

$$\frac{\partial D_x}{\partial t} = -\frac{\partial H_y}{\partial z} \ , \quad \mu_0 \frac{\partial H_y}{\partial t} = -\frac{\partial E_x}{\partial z} \ , \quad D_x = \epsilon_0 \epsilon_r E_x + P_x \ ,$$

where P_x is the induced polarization.

In the case of semiconductors, P_x is calculated by using the semiconductor Bloch equations [1], (a two band model, one conduction band and one valence band).

$$\frac{dn_k^e}{dt} = -\frac{n_k^e - \bar{n}_k^e}{\tau_e} - \frac{n_k^e - \bar{n}_k^e}{\tau_c} - 2Im(\Omega_k p_k^*) \ , \quad \frac{dn_k^h}{dt} = -\frac{n_k^h - \bar{n}_k^h}{\tau_e} - \frac{n_k^h - \bar{n}_k^h}{\tau_v} - 2Im(\Omega_k p_k^*) \ ,$$

$$\frac{dp_{1,k}}{dt} = -\frac{p_{1,k}}{\tau_2} + \Delta_k p_{2,k} + \Omega_{2,k} w_k \qquad \frac{dp_{2,k}}{dt} = -\frac{p_{2,k}}{\tau_2} - \Delta_k p_{1,k} - \Omega_{1,k} w_k$$

where n_k^e and n_k^h are the occupation probabilities for electron and holes of the wave vector k in the conduction and valence bands respectively, $w_k = (n_k^e + n_k^h - 1)$ is the population inversion, $p_{1,k}$ and $p_{2,k}$ are the dispersive and absorptive components of the dipole moment p_k, of the wave vector k, $p_k = p_{1,k} + ip_{2,k}$ and the τ parameters govern various decay processes. The transition energy $\hbar\omega_k$ is varied over a sufficiently large range to accurately describe the interaction of an ultrashort optical pulse with the semiconductor. $\bar{n}_k^e(t)$ and $\bar{n}_k^h(t)$

are determined by first computing the chemical potentials $\mu^e(t)$ and $\mu^h(t)$ from $n_k^e(t)$ and $n_k^h(t)$ respectively and then using the formula for a Fermi-Dirac distribution to find the quasi-equilibrium Fermi distributions $\bar{n}_k^e(t)$ and $\bar{n}_k^h(t)$

The generalized Rabi frequency $\Omega_k = \Omega_{1,k} + i\Omega_{2,k}$, the effective transition energy $\hbar\Delta_k$, which includes the band-gap renormalization, and the induced polarization P_x are given respectively by

$$\Omega_k = \frac{1}{\hbar}(\mu E_x(t) + \sum_{q \neq k} V_{|k-q|} p_q), \quad \hbar\Delta_k = \hbar\omega_k - \sum_{q \neq k} V_{|k-q|}(n_q^e + n_q^h), \quad P_x(t) = \frac{2\mu}{\pi^2}\int_0^\infty p_{1,k} k^2 dk$$

Initially an algorithm was developed for the simpler optical Maxwell-Block equations for two-level atomic systems [7]. A calculation of self-induced transparency was made for a a 10 fs pulse [8]. Figure 1 shows the electric field of the pulse at several moments during its propagation inside the medium. The top curve on the right side in figure 2 shows the corresponding population inversion at some location as the pulse goes by. The top curve on the left side in figure 2 shows the resulting population inversion for self-induced transparency when the SVEA and the RWA are made. The remaining curves are a comparison of the two methods when the atomic transition frequency is detuned away from the optical carrier frequency. The exact method is able to capture the off resonance details that the approximate method is incapable of modeling.

Next the semiconductor Maxwell-Block equations were solved [8] under the simplifications that the Coulomb interaction terms were neglected (the free carrier assumption) and that there were no relaxation terms in the equations for the evolution of n_k^e and n_k^h. Figures 3-6 show colliding pulses, including constructive and destructive interference. Figure 7 shows gain curves that were obtained under the free carrier assumption.

Finally figure 8 shows exciton results. Notice the 1s and 2s absorption peaks in the case of the 2 ps dipole decay time. Here the population inversion was specified at minus one, the generalized Rabi frequency was used but the transition energy was not renormalized. The presentation shall include additional calculations of propagating and colliding pulses in which all the Coulomb and relaxation terms are included.

We would like to thank Rolf Binder, Optical Sciences Center, University of Arizona, for his many helpful comments concerning algorithm development for the semiconductor Bloch equations.

References

1. Haug, H., and Koch, S. W., *Quantum Theory of the Optical and Electronic Properties of Semiconductors* , World Scientific Press, 2nd Ed., 1993.
2. Goorjian, P. M. and Taflove, A.,"Direct Time Integration of Maxwell's Equations in Nonlinear Dispersive Media for Propagation of Femtosecond Electromagnetic Solitons," *Optics Letters* , Vol. 17, No. 3, Feb. 1, 1992.
3. Goorjian, P. M., Taflove, A., Joseph, R. M., and Hagness, S. C., "Computational Modeling of Femtosecond Optical Solitons from Maxwell's Equations," *IEEE Journal of Quantum Electronics* , special issue on "Ultrafast Optics and Electronics," vol. 28, No. 10, pp. 2416-2422, Oct., 1992.
4. Goorjian, P. M. and Silberberg, Y.: "Numerical simulation of light bullets, using the full vector, time dependent Maxwell equations," Nonlinear Optics Topical Meeting, Waikoloa, Hawaii, July 24-29, 1994 and Integrated Photonics Research Topical Meeting, (IPR'95), February 23-25, 1995, at Dana Point, CA., both cosponsored by Optical Society of America and IEEE/Lasers and Electro-Optics Society.
5. Silberberg, Y.: "Collapse of optical pulses," *Optics Letters*, Vol. 22, pp. 1282-1284, November 15, 1990.
6. Flesch, R. G., Pushkarev, A. and Moloney, J. V.: "Carrier Wave Shocking of Femtosecond Optical Pulses," *Phy. Rev. Lett.*, Vol. 76, No. 14, pp. 2488-2499, April 1, 1996.
7. Allen, L. and Eberly, J. H., *Optical Resonance and Two-Level Atoms* , Dover Press, 1987.
8. Goorjian, P. M. and Agrawal, G. P.: "Computational Modeling of Ultrashort Optical Pulse Propagation in Nonlinear Optical Materials," Paper NME31, Nonlinear Optics Topical Meeting, Maui, HI, July 8-12, 1996

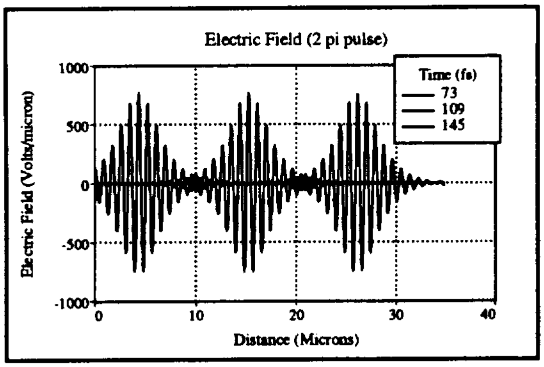

Fig. 1. Two-level atom. Self induced transparency.

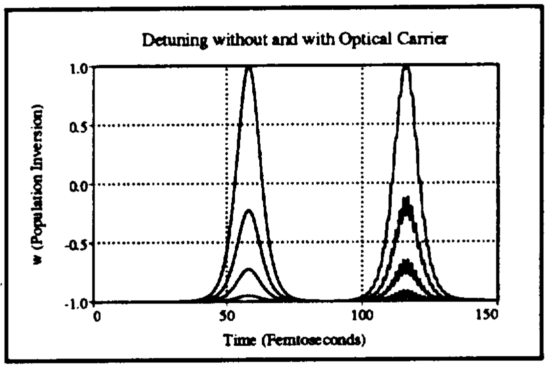

Fig. 2. Two-level atom. Population inversion.

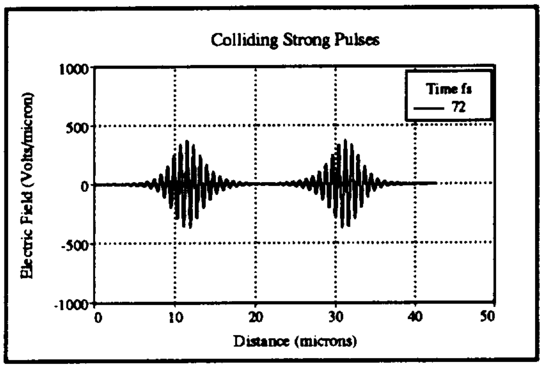

Fig. 3. Approaching Pulses

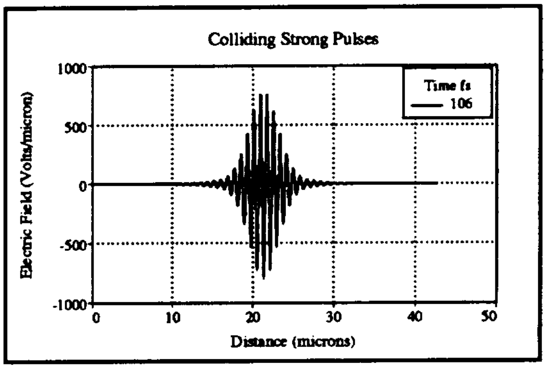

Fig. 4. Constructive Interference

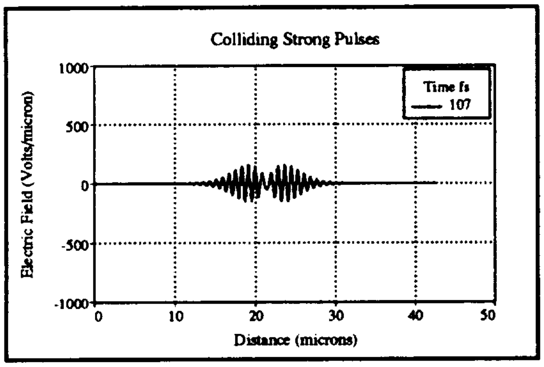

Fig. 5. Destructive Interference

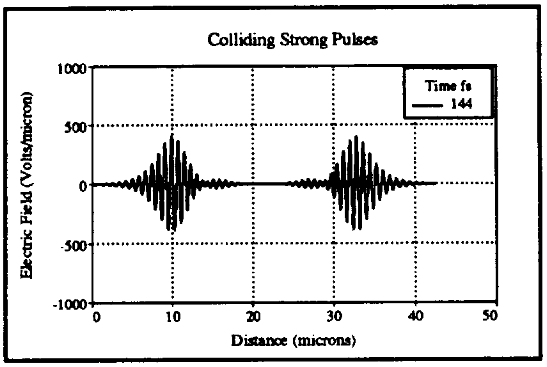

Fig. 6. Separating Pulses

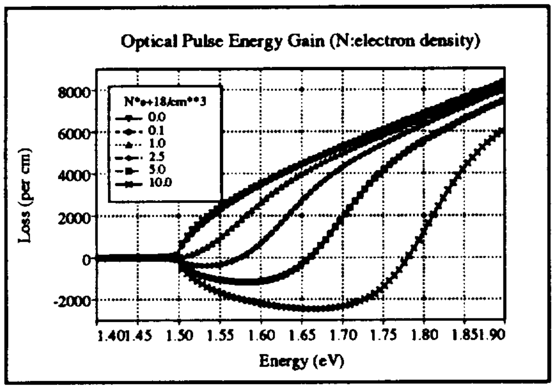

Fig. 7. Gain Curves

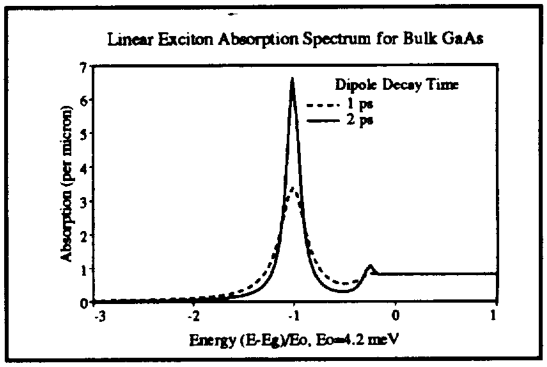

Fig. 8. Exciton Absorption Spectrum

Maxwell–Bloch dynamics and modulation instabilities in fiber lasers and amplifiers

Guido H. M. van Tartwijk and Govind P. Agrawal

The Institute of Optics and Rochester Theory Center, University of Rochester, Rochester, New York 14627

Received January 31, 1997; revised manuscript received March 24, 1997

We investigate analytically the occurrence of modulation instability in doped fiber lasers and amplifiers using a Maxwell–Bloch description for the dopants and without making the usual parabolic-gain approximation. We find a new modulation instability occurring near the Rabi frequency, which is not predicted by the conventional complex Ginzburg–Landau model. We discuss the implications of this new instability for fiber amplifiers and lasers and analyze the effects of the saturable host absorption on the laser instabilities. Atomic detuning is shown to significantly enhance the new modulation instability, in both the normal- and the anomalous-dispersion regimes. © 1997 Optical Society of America [S0740-3224(97)04610-9]

1. INTRODUCTION

The onset of instabilities in various kinds of lasers is generally studied by use of a rate-equation model based on the Maxwell–Bloch equations suitable for a two-level atomic system.[1] Such a model, often referred to as the (detuned) Lorenz–Haken model, includes atomic polarization dynamics and has been used extensively over the past two decades. Its use leads to the concept of the second laser threshold, defined as the pump level at which the continuous-wave (cw) operation of the laser becomes unstable through a Hopf bifurcation, resulting in a self-pulsing output. At higher pump levels the laser can enter into a chaotic regime through a period doubling or another route to chaos.[1,2]

The advent of fiber lasers during the late 1980's forces several changes to this standard model of laser instabilities, mainly because the optical fiber, acting as a host to the dopants, introduces group-velocity dispersion (GVD) and self-phase modulation (SPM), both of which must be incorporated for a proper description of the onset of instabilities in fiber lasers.[3] In fact, these two phenomena lead to an instability, known as the modulation instability (MI), even in an undoped and unpumped optical fiber.[4] It is therefore reasonable to expect that the presence of GVD and SPM in the host fiber would change the nature of instabilities in fiber lasers in comparison with other kinds of lasers (gas and solid-state lasers) that are well described by the standard Lorenz–Haken model. Apart from this propagation-based instability, several other explanations for the observed instabilities in rare-earth-doped fiber lasers have been reported. It was shown theoretically and experimentally that the existence of ion clusters in heavily Er-doped fiber lasers leads to single-mode cw or self-pulsing behavior, whereas the same model is also applicable to dual-wavelength or bipolarized lasers.[5,6] Other theories and experiments on Er-doped fiber lasers have shown self-pulsing, chaos, and antiphase dynamics between the different polarization eigenstates of the optical field.[7,8] The explanation for the self-pulsing behavior of Nd-doped fiber lasers has been reported to be driven by the dynamics of the two field-polarization eigenstates that depend on the birefringence of the fiber.[9,10] In this paper, however, we focus on the propagation-driven MI phenomenon, and do not consider any field-polarization dynamics.

In recent years, the MI phenomenon has been investigated in doped (active) fibers used to make lasers and amplifiers.[3,4,11,12] When doing so, one has to consider the nonlinear interaction of the dopants with the optical field. A natural choice is to model the dopants as a two-level system with an atomic polarization dephasing time T_2 and a population relaxation time T_1. By far, the most popular model employs the parabolic-gain approximation, leading to a complex Ginzburg–Landau (CGL) equation for the optical field.[3] One study showed that in erbium-doped fiber amplifiers,[11] the threshold for MI is considerably lowered compared with that for undoped fibers. Recently, Chen *et al.*[12] included gain dynamics (governed by T_1) as well as a fast saturable absorber in the model and discussed the implications of MI for passively mode-locked figure-eight lasers. The full atomic polarization dynamics (governed by T_2) has, however, been neglected so far.

In this paper we investigate the occurrence of MI beyond the Ginzburg–Landau approximation by considering the full T_2 dynamics. We introduce the theoretical framework in Section 2 and discuss the consequences for amplifiers in Section 3. There, we calculate the steady-state solutions and derive a dispersion relation for MI. The effect of the population relaxation damping time T_1 and the dipole dephasing time T_2 on MI are studied for amplifiers. We find that by cooling the fiber amplifier, the bandwidth and the strength of the MI can be greatly reduced. In Section 4 we deal with fiber lasers and derive the dispersion relation for MI at resonance. The role of saturable absorption in fiber lasers is investigated, and we focus on the possibility of MI occurring in the normal-dispersion regime. We find indeed such an instability, having its origin in the atomic coherence effects related to the atomic polarization dynamics. This new instability is found to occur at rather low frequencies (~50 MHz) and

may explain the self-starting behavior of mode-locked Nd-doped lasers. In Section 5 we discuss the effects of detuning on the occurrence of MI and discuss the differences between normal and anomalous operating regimes.

2. THEORETICAL FRAMEWORK

Our starting point is a set of Maxwell–Bloch equations that describe the propagation of optical fields in a nonlinear, dispersive medium doped with two-level atoms (or ions). We write the electrical field $\mathscr{E}(x, y, z, t)$ and the induced material polarization $\mathscr{P}(x, y, z, t)$ as

$$\mathscr{E}(x, y, z, t) = \tfrac{1}{2}\hat{x}F(x, y)A(z, t) \times \exp[i(\beta_0 z - \omega_0 t)] + \text{c.c.}, \quad (1)$$

$$\mathscr{P}(x, y, z, t) = \tfrac{1}{2}\hat{x}F(x, y)B(z, t) \times \exp[i(\beta_0 z - \omega_0 t)] + \text{c.c.}, \quad (2)$$

where $\hat{x}$ is the polarization unit vector of the light assumed to be linearly polarized along the x axis, $F(x, y)$ is the fiber-mode profile, and β_0 is the wave number corresponding to the carrier frequency ω_0. We assume that the field-polarization direction is preserved upon propagation and that we are dealing with a polarization-preserving single-mode fiber. However, most of the results are expected to remain qualitatively valid for conventional optical fibers. After substituting Eqs. (1) and (2) into Maxwell's equations, and making the slowly-varying-envelope and rotating-wave approximations, we obtain the following equations for the slowly varying complex amplitudes A and B (Ref. 4):

$$\frac{\partial A}{\partial z} = \frac{i}{2}B - \frac{1}{2}\alpha A - \frac{i\beta_2}{2}\frac{\partial^2 A}{\partial t^2} + (\theta + i\gamma)|A|^2 A, \quad (3)$$

$$T_2\frac{\mathrm{d}B}{\mathrm{d}t} = (i\delta - 1)B - iAg, \quad (4)$$

$$T_1\frac{\mathrm{d}g}{\mathrm{d}t} = g_0 - g + \mathrm{Im}(A^*B)/P_{\mathrm{sat}}, \quad (5)$$

where g is the gain realized by pumping the dopants, α is the optical loss, β_2 is the GVD coefficient of the host fiber, θ accounts for saturable host absorption, γ is the fiber nonlinearity, $\delta = (\omega_0 - \bar{\omega})T_2$ is the scaled detuning between the carrier frequency ω_0 and the atomic resonance frequency $\bar{\omega}$, g_0 is the unsaturated gain, and P_{sat} is the saturation power for the dopants modeled as a homogeneously broadened two-level system. We have written Eqs. (3)–(5) in such a way that A has units of $\sqrt{W}$, B has units of $\sqrt{W}L^{-1}$, and g has units of L^{-1}, where L is the length of either the amplifier or the laser cavity.

It is important to note that Eqs. (3)–(5) are based on a traveling-wave description rather than a standing-wave approach that is employed in the conventional rate-equation analysis. Since we adopt a traveling-wave approach, the optical field $A(z, t)$ in Eqs. (3)–(5) in principle can represent a very wide spectrum (or many longitudinal modes). The detuning parameter δ is thus interpreted as the mismatch between the gain peak and the dominant frequency of the laser spectrum. The main assumptions in our model are the homogeneously broadened gain medium and the neglect of spontaneous emission. The former is not valid for all doped fibers, but for some types of glass hosts it is a reasonable assumption.[4] Since we are interested in deterministic instabilities, spontaneous emission can be neglected without loss of generality.

There are two distinct origins of the nonlinear effects in Eqs. (3)–(5). The fiber nonlinearity $\gamma = n_2\omega_0/cA_{\mathrm{eff}}$ accounts for SPM effects induced by the host, where n_2 is the nonlinear refractive index (units m^2/W), c is the speed of light in vacuum, and A_{eff} is the effective fibercore area. For completeness we give the relation between n_2 and the nonlinear susceptibility $\tilde{\chi}^{(3)}$ (units of meters squared per volt squared) of the fiber

$$n_2 \equiv \frac{3}{4\epsilon_0 n^2 c}\,\mathrm{Re}[\tilde{\chi}^{(3)}(\omega_0)], \quad (6)$$

where n is the background refractive index and ϵ_0 is the permittivity of the vacuum. The dopant-induced nonlinear effects are governed by the saturation power P_{sat}, defined as

$$P_{\mathrm{sat}} \equiv \frac{\hbar^2 c n \epsilon_0 A_{\mathrm{eff}}}{2\mu^2 T_1 T_2}, \quad (7)$$

where $\hbar$ is Planck's constant divided by 2π and μ is the dipole moment of the atomic transition. Note that Eqs. (3)–(5) are written in the frame of reference moving with group velocity $v_g \equiv \beta_1^{-1}$, which means that $t = T - \beta_1 z$, where T is the time in the rest frame. By doing this, we eliminate the term $\beta_1(\partial A/\partial T)$ from the left-hand side of Eq. (3).

We now briefly discuss the relation of Eqs. (3)–(5) with the CGL model.[4,12] When the assumption is made that the population relaxation time T_1 is much longer than all other lifetimes, we can approximate the actual gain g by its steady-state value g_s. This allows Eq. (4) to be expressed in the Fourier domain as the well-known Lorentzian-shaped nonlinear susceptibility:

$$\frac{\tilde{B}(\Delta\omega)}{\tilde{A}(\Delta\omega)} = \frac{-ig_s}{1 - i(\Delta\omega T_2 + \delta)}, \quad (8)$$

where $\Delta\omega = \omega - \omega_0$ is the detuning of the spectral component from the carrier frequency. In the CGL model, polarization equation (8) is approximated by a Taylor expansion near $\Delta\omega = 0$ up to second order, leading to the parabolic-gain approximation that is reasonably accurate for small values of T_2. In the time domain this corresponds to (generally complex) corrections $\Delta\beta_1$ and $\Delta\beta_2$ of the inverse group velocity β_1 and the GVD coefficient β_2 (Ref. 3):

$$\Delta\beta_1(\delta) = \frac{1}{2}g_2 T_2 \frac{1}{(1 - i\delta)^2}, \quad (9)$$

$$\Delta\beta_2(\delta) = g_s {T_2}^2 \frac{i}{(1 - i\delta)^3}. \quad (10)$$

From Eq. (9) we see that only at resonance ($\delta = 0$) can the resulting pulse propagation equation be written in the reference frame moving with the new group velocity (β_1

$+ \Delta\beta_1)^{-1}$, because only at resonance is the correction $\Delta\beta_1$ real. After writing the correction to the GVD as $\Delta\beta_2(0) = ib \equiv ig_s T_2{}^2$, the resulting equations of the CGL model become

$$\frac{\partial A}{\partial z} = \frac{1}{2}(g - \alpha)A + \frac{1}{2}(b - i\beta_2)\frac{\partial^2 A}{\partial t^2} + (\theta + i\gamma)|A|^2 A, \qquad (11)$$

$$T_1 \frac{\mathrm{d}g}{\mathrm{d}t} = g_0 - g - \frac{g|A|^2}{P_{\mathrm{sat}}}. \qquad (12)$$

Obviously, Eqs. (11) and (12) are good approximations of the full model only if T_1 is long enough and T_2 is short enough. In this paper we explore the shortcomings of the CGL model for realistic fiber lasers and amplifiers and find interesting behavior outside the realm of the CGL model. We note that the CGL model is only useful for amplifiers for which gain saturation can be neglected; otherwise, the gain dispersion b would be z dependent, which seems impractical at best.

The Maxwell–Bloch equations (3)–(5) can be applied to both amplifiers and unidirectional (e.g., ring) lasers. In the case of lasers, however, one should, in general, solve a complicated boundary-value problem to account for the localized losses at the cavity mirrors, a task that requires a numerical approach. In this paper we adopt the mean-intensity approximation by replacing the localized mirror losses with a distributed loss incorporated in the total optical loss α. In the case of amplifiers, such a mean-intensity requirement is not valid: the intensity is strongly z dependent. Because the steady states are so different for lasers and amplifiers, a modulation stability analysis yields very different results. In the following, we treat them separately.

3. MODULATION INSTABILITY IN AMPLIFIERS

We consider an amplifier (or absorber) of length L with an input power P_0 at $z = 0$. We first find the time-independent (steady-state) solution of Eqs. (3)–(5). Formally, it can be written as

$$A_s(z) = [P_A(z)]^{1/2}\exp[i\varphi_s(z)], \qquad (13)$$

$$B_s(z) = \frac{A_s(z)g_s(z)}{\delta + i}, \qquad (14)$$

$$g_s(z) = g_0\left[1 + \frac{P_A(z)}{P_{\mathrm{sat}}(1 + \delta^2)}\right]^{-1}. \qquad (15)$$

Using the imaginary part of Eq. (3), we can write the phase profile $\varphi_s(z)$ in terms of the power profile $P_A(z)$:

$$\varphi_s(z) = \gamma\int_0^z \mathrm{d}z' P_A(z') + \frac{\delta/2}{1 + \delta^2}\int_0^z \mathrm{d}z' g_s(z'). \qquad (16)$$

From the real part of Eq. (3), and using Eq. (15), one finds the following differential equation for the scaled power profile $f(z) \equiv P_A(z)/[P_{\mathrm{sat}}(1 + \delta^2)]$:

$$\frac{\mathrm{d}f}{\mathrm{d}z} = \frac{g_0}{1 + \delta^2}\frac{f}{f + 1} - \alpha f + 2\theta P_{\mathrm{sat}}(1 + \delta^2)f^2. \qquad (17)$$

This differential equation can be solved, resulting in following transcendental equation for P_A:

$$\begin{aligned} 2\theta P_{\mathrm{sat}}(1 + \delta^2)z &= -\left(\frac{C}{C_+} + \frac{1 - C}{C_-}\right)\ln\left[\frac{P_A(z)}{P_0}\right] \\ &+ \frac{C}{C_+}\ln\left[\frac{P_A(z) - C_+P_{\mathrm{sat}}(1 + \delta^2)}{P_0 - C_+P_{\mathrm{sat}}(1 + \delta^2)}\right] \\ &+ \frac{1 - C}{C_-}\ln\left[\frac{P_A(z) - C_-P_{\mathrm{sat}}(1 + \delta^2)}{P_0 - C_-P_{\mathrm{sat}}(1 + \delta^2)}\right], \qquad (1 \end{aligned}$$

where the coefficients C and $C_\pm$ are given by

$$C = \frac{1 + C_+}{C_+ - C_-},$$

$$2C_\pm = c_2 - 1 \pm [(1 - c_2)^2 - 4(c_1 - c_2)]^{1/2}, \qquad (1$$

$$c_1 = \frac{g_0}{2\theta P_{\mathrm{sat}}(1 + \delta^2)^2}, \quad c_2 = \frac{\alpha}{2\theta P_{\mathrm{sat}}(1 + \delta^2)}. \qquad (2$$

In the absence of saturable absorption ($\theta = 0$), the solution of Eq. (17) is implicitly given by

$$\begin{aligned} \left(\frac{g_0}{1 + \delta^2} - \alpha\right)z &= \ln\left[\frac{P_A(z)}{P_0}\right] - \frac{g_0}{\alpha(1 + \delta^2)} \\ &\times \ln\left\{\frac{P_A(z) - P_{\mathrm{sat}}(1 + \delta^2)\left[\frac{g_0}{\alpha(1 + \delta^2)} - 1\right]}{P_0 - P_{\mathrm{sat}}(1 + \delta^2)\left[\frac{g_0}{\alpha(1 + \delta^2)} - 1\right]}\right\}, \end{aligned} \qquad (21)$$

which, in the absence of optical loss ($\alpha = 0$), reduces to

$$\ln\left[\frac{P_A(z)}{P_0}\right] + \frac{P_A(z) - P_0}{P_{\mathrm{sat}}} = \frac{g_0 z}{1 + \delta^2}. \qquad (22)$$

After the power profile $P_A(z)$ is found, the gain profile $g_s(z)$ and the polarization profile $B_s(z)$ follow from Eqs. (13)–(16).

To study the onset of MI, we follow a standard approach[4] by considering the linear stability of the steady-state (cw) solution given above. Considering small perturbations u, v, p, q, and x from the cw state defined as

$$A(z, t) = [(P_0)^{1/2} + u(z, t) + iv(z, t)] \times \left[\frac{P_A(z)}{P_0}\right]^{1/2} \exp[i\varphi_s(z)], \tag{23}$$

$$B(z, t) = \frac{g_s(z)}{\delta + i}[(P_0)^{1/2} + p(z, t) + iq(z, t)] \times \left[\frac{P_A(z)}{P_0}\right]^{1/2} \exp[i\varphi_s(z)], \tag{24}$$

$$g(z, t) = [g_0 + x(z, t)]\left[1 + \frac{P_A(z)}{P_{\mathrm{sat}}(1 + \delta^2)}\right]^{-1}, \tag{25}$$

and linearizing Eqs. (3)–(5) in u, v, p, q, and x, we solve the resulting five linear equations in Fourier space by introducing

$$y(z, t) = y_0 \exp\left[i \int \mathrm{d}z K(z) - i\Omega t\right], \qquad y = u, v, p, q, x, \tag{26}$$

where y_0 is the initial amplitude, Ω is the frequency, and $K(z)$ is the local wave number of the perturbation. The resulting dispersion relation for arbitrary detuning δ is discussed for fiber lasers in Section 5. The dispersion relation at resonance ($\delta = 0$) is given by

$$\begin{aligned}\{&[2iK(z) + g_s(z) - 4\theta P_A(z)][2iK(z) + g_s(z)]\\ &+ \beta_2{}^2\Omega^2[\Omega^2 + \mathrm{sgn}(\beta_2)\Omega_c{}^2(z)]\}(1 - i\Omega T_2)\\ &\times [(1 - i\Omega T_1)(1 - i\Omega T_2) + I(z)]\\ &- g_s(z)[2iK(z) + g_s(z)](1 - i\Omega T_2)\\ &\times [1 - i\Omega T_1 - I(z)] - g_s(z)\\ &\times [2iK(z) + g_s(z) - 4\theta P_A(z)]\\ &\times [(1 - i\Omega T_1)(1 - i\Omega T_2) + I(z)]\\ &+ g_s{}^2(z)[1 - i\Omega T_1 - I(z)] = 0,\end{aligned} \tag{27}$$

where $I(z) = P_A(z)/P_{\mathrm{sat}}$, $\mathrm{sgn}(\beta_2) = \pm 1$, and $\Omega_c(z) = [4\gamma P_A(z)/|\beta_2|]^{1/2}$ is the critical frequency, i.e., the maximum frequency for which MI is found to occur in the case of anomalous dispersion in a passive fiber.[4] Before we examine the implications of Eq. (27) in various regimes of parameter space, we note that the Rabi frequency is somewhat hidden:

$$\Omega_{\mathrm{Rabi}}(z) \equiv \left[\frac{P_A(z)}{P_{\mathrm{sat}} T_1 T_2}\right]^{1/2}. \tag{28}$$

The imaginary part of $K(z)$ determines the local gain experienced by the perturbation. It is useful to define the total integrated gain at frequency Ω as[11]

$$h(\Omega) \equiv -2 \int_0^L \mathrm{d}z\ \mathrm{Im}[K(\Omega, z)], \tag{29}$$

where the factor 2 converts $h(\Omega)$ to power gain. MI occurs whenever the wave number K has a negative imaginary part. In the case of an amplifier, this means the perturbation grows faster than the steady-state power, whereas for an absorber it means that the perturbation dampens less quickly. Dispersion equation (27) reduces to the previously reported ones in the appropriate limits. In the absence of saturable host absorption ($\theta = 0$), the dispersion relation from Ref. 11 is obtained in the limit of large T_1 and short T_2.

We now consider the occurrence of MI in various regimes of parameter space for both amplifiers and absorbers. Because our model has no restrictions with respect to the magnitude of the lifetimes T_1 and T_2, we can explore MI in regimes where the CGL model has no validity. For simplicity, we only consider the local perturbation gain because the integration in Eq. (29) can be performed analytically in a few limiting cases only.[3] We also ignore the possibility of saturable host absorption since two-photon absorption is relatively weak in silica fibers, and other sources of saturable nonlinearity are rarely present in amplifiers. When we discuss MI in lasers, we show how even relatively small amounts of saturable host absorption can affect the MI drastically.

We start by investigating the effect of the magnitude of the dipole lifetime T_2. For most fiber amplifiers, T_2 is estimated to be near 100 fs, corresponding to a wide gain spectrum. Because T_1 is usually in the range 0.1–10 ms, the CGL equation is expected to be a good approximation. However, by cooling the fiber, the polarization dephasing process can be slowed down substantially, making values of $T_2 \sim 10$ ps readily attainable.[13]

In Fig. 1 we show for various values of T_2 in the range 0.1–10 ps the MI spectrum for a typical fiber amplifier with a 30-dB gain, i.e., $\exp(g_0 L) = 1000$. All other parameters are given in the caption. Note that the saturation power P_{sat} is inversely proportional to T_2 [Eq. (7)]. When Eq. (7) is satisfied for each value of T_2, the Rabi frequency remains a constant for all curves: $\Omega_{\mathrm{Rabi}} = 1.29 \times 10^{-3}\Omega_c$. When the dephasing time T_2 is increased, two trends are observed.

First, as can be seen in Fig. 1, increasing T_2 leads to a shrinkage of the MI bandwidth, whereas the maximum

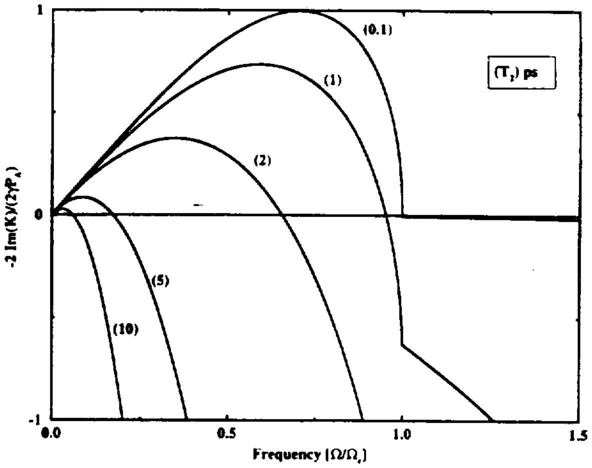

Fig. 1. Modulation instability spectrum for an erbium-doped fiber amplifier at various values of T_2 (indicated in the figure). Parameters are $g_0 = 6.91\,\mathrm{L}^{-1}$, $P_0 = 1\,\mathrm{mW}$, $T_1 = 0.1\,\mathrm{ms}$, $\beta_2 = -20\,\mathrm{ps}^2/\mathrm{L}$, $\gamma = 3W^{-1}\,\mathrm{L}^{-1}$, and $P_{\mathrm{sat}} = 1\,\mathrm{mW}$ when $T_2 = 0.1\,\mathrm{ps}$. For undoped fibers, MI occurs up to $\Omega_{\mathrm{crit}}/2\pi = 3.9\,\mathrm{GHz}$

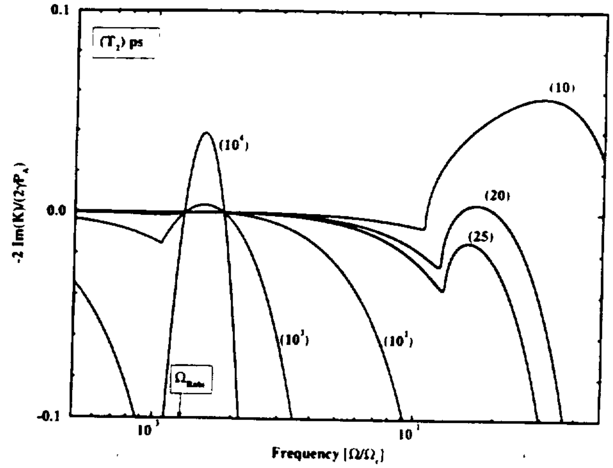

Fig. 2. MI spectrum for the amplifier of Fig. 1, for even longer dephasing times T_2 (indicated in the figure). In the range $21 < T_2 < 80$ ps, MI is totally quenched. When T_2 approaches 100 ps, the MI spectrum starts to show a narrow, weak peak around the Rabi frequency $\Omega_{\mathrm{Rabi}}/\Omega_c = 0.0013$.

gain within the bandwidth decreases rapidly. When $T_2 = 100$ fs ($P_A/P_{\mathrm{sat}} = 0.01$), MI occurs for frequencies up to $\Omega_c/2\pi = 3.9$ GHz, while the peak MI strength is found near $\Omega = \Omega_c/\sqrt{2}$. The peak strength is very close to the analytical value $2\gamma P_A$, which is found in the CGL limit.[11] Already when $T_2 = 2$ ps ($P_A/P_{\mathrm{sat}} = 0.2$), the frequency band where MI occurs has shrunk ~40%, and near $T_2 = 8$ ps ($P_A/P_{\mathrm{sat}} = 0.8$), MI has almost ceased to occur at all. Near $T_2 = 21$ ps ($P_A/P_{\mathrm{sat}} = 2.1$), the MI band vanishes completely. Long before that happens, the strength of MI is so weak that it is doubtful whether it can be observed in a single-pass amplifier.

Second, during this MI spectrum shrinkage, another phenomenon is occurring that is directly caused by the two-level system since it involves frequencies close to Ω_{Rabi}, as is shown in Fig. 2. Near the Rabi frequency a secondary, weak maximum in MI strength begins to form for $T_2 > 20$ ps. This maximum becomes positive near $T_2 = 80$ ps ($P_A/P_{\mathrm{sat}} = 8$) and grows with T_2. When T_2 is increased further, the MI spectrum slowly returns to its original width and strength (out of scale in Fig. 2). Near $T_2 = 11.5$ ns ($P_A/P_{\mathrm{sat}} = 1150$), the MI spectrum shows again positive MI gain around Ω_c, while maintaining a narrow (but weak) peak close to Ω_{Rabi}. At the highly improbable value of $T_2 \sim 1\ \mu$s ($P_A/P_{\mathrm{sat}} = 10^5$) the MI spectrum is very close to the one at $T_2 = 100$ fs, and we have come full circle.

Thus we find four regimes of T_2: in the first regime ($100\text{ fs} < T_2 < 21$ ps), increasing T_2 leads to a total quenching of MI. In the second regime ($21\text{ ps} < T_2 < 80$ ps), no MI occurs, but the gain around the Rabi frequency is growing. In the third regime ($80\text{ ps} < T_2 < 11.5$ ns), more and more MI occurs around the Rabi frequency, while the gain around Ω_c is growing toward a positive value again. In the fourth regime, approaching the long T_2 limit ($1\ \mu\text{s} < T_2 < \infty$), the MI spectrum recovers fully to its original (small T_2) form. The boundaries between these regimes are, of course, strongly dependent on the power level P_A. For higher power levels these boundaries rapidly decrease.

We further note that the MI band near Ω_c is insensit to changes in T_1, as long as it is accompanied by a chan in the saturation power P_{sat} according to Eq. (7). Ho ever, if we keep the saturation power constant up changing T_1 (this can be done by adjusting the dipole n ment μ), decreasing T_1 leads to a stabilization of t lower frequencies and eventually a reduction of MI alt gether.

We emphasize that the narrow MI peak around Ω_{Rab} so weak that it is questionable whether it can be observ in an amplifier. In the case of a laser, however, such weak gain may build to a substantial instability ov many round trips, as we discuss in the next sectio Since it is not common to use an amplifier in the high saturated regime, the emergence of the narrow MI bar near the Rabi frequency is not very practical. Note, ho ever, that this narrow MI band near the Rabi frequen does not depend on the sign of β_2; in both normal- an anomalous-dispersion regimes, this instability emerges a relatively high values of T_2.

Apart from this new (and for realistic systems, ex tremely weak) instability, the full Maxwell–Bloch mod agrees with the CGL model qualitatively rather well. O course, the quantitative differences become larger as th approximations leading to the CGL model (large T_1 an short T_2) become more and more inappropriate. In th next section we find that for lasers the situation can b very different.

4. MODULATION INSTABILITY IN FIBER LASERS AT RESONANCE

Equations (3)–(5) also describe the optical field and the gain in a laser, when one assumes that all losses can be thought of as being distributed along the cavity. Then, the steady-state solution is characterized by a z-independent power P_0 and gain g_s, and can be written as

$$A_s(z) = (P_0)^{1/2} \exp[i\varphi_s(z)], \tag{30}$$

$$B_s(z) = \frac{\delta - i}{1 + \delta^2} A_s g_s, \tag{31}$$

$$g_s = g_0 \left[1 + \frac{P_0}{P_{\mathrm{sat}}(1 + \delta^2)} \right]^{-1}. \tag{32}$$

Again, from the real and the imaginary part of Eq. (3), the following expressions for the laser power P_0 and the phase profile $\varphi_s(z)$ are obtained:

$$g_s = (\alpha - 2\theta P_0)(1 + \delta^2), \tag{33}$$

$$\frac{\mathrm{d}\varphi_s}{\mathrm{d}z} = \gamma P_0 + \frac{1}{2}\left(\frac{\delta g_s}{1 + \delta^2} - \alpha \right). \tag{34}$$

Since Eq. (33) is quadratic in P_0 [with use of Eq. (32)], in principle, two values for the laser power are found. One of these is not physical and corresponds to the antilaser, which is characterized by a huge gain and almost zero power.

Similar to the amplifier case, we consider small perturbations u, v, p, q, and x from the cw state, defined as

$$A(z, t) = [(P_0)^{1/2} + u(z, t) + iv(z, t)]\exp[i\varphi_s(z)], \tag{35}$$

$$B(z, t) = \frac{\delta - i}{1 + \delta^2}[(P_0)^{1/2} + p(z, t) + iq(z, t)]g_s\exp[i\varphi_s(z)], \tag{36}$$

$$g(z, t) = [g_0 + x(z, t)]\left[1 + \frac{P_0}{P_{\text{sat}}(1 + \delta^2)}\right]^{-1}, \tag{37}$$

and linearizing Eqs. (3)–(5) in u, v, p, q, and x, we solve the resulting five linear equations in the Fourier space by introducing

$$y(z, t) = y_0 \exp[i(Kz - \Omega t)], \quad y = u, v, p, q, x, \tag{38}$$

where y_0 denotes the initial amplitude of the perturbation. Note that because because both laser power P_0 and g_s are z independent, the wave number K is also z independent. At resonance ($\delta = 0$), the resulting dispersion relation reads

$$\begin{aligned}\{[2iK + \alpha - 6\theta P_0](2iK + \alpha - 2\theta P_0) &\\ + \beta_2{}^2\Omega^2[\Omega^2 + \text{sgn}(\beta_2)\Omega_c{}^2]\}(1 - i\Omega T_2) &\\ \times [(1 - i\Omega T_1)(1 - i\Omega T_2) + I_0] &\\ - g_s(2iK + \alpha - 2\theta P_0)(1 - i\Omega T_2) &\\ \times [1 - i\Omega T_1 - I_0] - g_s(2iK + \alpha - 6\theta P_0) &\\ \times [(1 - i\Omega T_1)(1 - i\Omega T_2) + I_0] &\\ + g_s{}^2(1 - i\Omega T_1 - I_0) = 0.\end{aligned} \tag{39}$$

Here, $I_0 = P_0/P_{\text{sat}}$, $\text{sgn}(\beta_2) = \pm 1$, and $\Omega_c = (4\gamma P_0/|\beta_2|)^{1/2}$ is the critical frequency, i.e., the maximum frequency for which MI is found in the case of anomalous dispersion in a passive fiber.[4] This dispersion relation is identical to Eq. (27) when one replaces K, P_0, and g_s by their z-dependent counterparts, and Eq. (33) is used.

Dispersion relation (39) reduces to the one previously reported by Chen *et al.*,[12] who employ the CGL model, in the appropriate limit.

Before we proceed with examining the implications of Eq. (39) in various regimes of parameter space, we note that the Rabi frequency is now given by

$$\Omega_{\text{Rabi}} \equiv \left(\frac{P_0}{P_{\text{sat}}T_1T_2}\right)^{1/2}. \tag{40}$$

Merely comparing the relative strengths of the critical frequency Ω_c with the Rabi frequency Ω_{Rabi} does not provide much information about the effect of atomic coherence on MI. The interaction between the fiber nonlinearity, the GVD, and the two-level system is much more involved.

In contrast with the amplifier case described in the previous section, lasers generally operate in the heavily saturated regime. This means that the instability near the Rabi frequency is now more likely to play a significant role. Furthermore, many fiber laser systems, e.g., a figure-eight laser, contain an effective saturable absorber that causes mode locking.

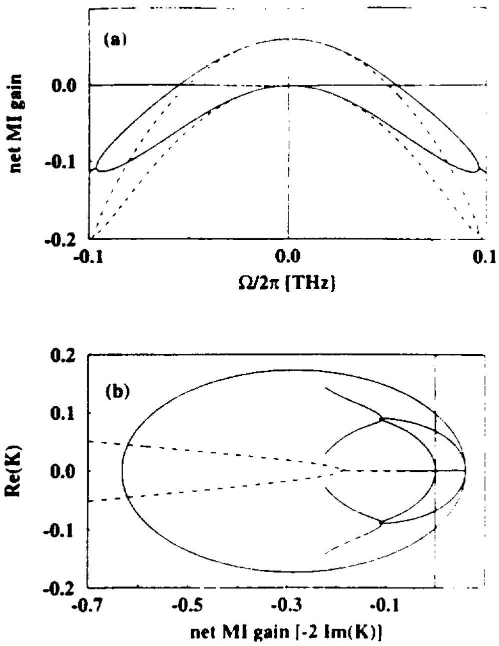

Fig. 3. MI analysis for a figure-eight laser. Solid curves indicate the results of the full model, while dashed curves show those of the CGL model. Top figure shows the net MI gain spectra, while the bottom figure shows the corresponding trajectory of the eigenvalue K on the complex plane. Parameters are $\alpha = 0.4\,\text{L}^{-1}$, $g_0 = 6\,\text{L}^{-1}$, $\beta_2 = -0.09\,\text{ps}^2\,\text{L}^{-1}$, $\theta = 0.1\,\text{W}^{-1}\,\text{L}^{-1}$, $\gamma = 0.008\,\text{W}^{-1}\,\text{L}^{-1}$, $T_2 = 1.27$ ps, $T_1 = 10^6$ ps, and $P_{\text{sat}} = 10$ mW.

We first compare the predictions of Eq. (39) with the CGL-based expression.[12] To facilitate comparison, we used the same parameters as in Ref. 12. In Fig. 3 we show the differences for the case of a figure-eight laser. Although the trajectories of K in the complex plane as a function of frequency Ω are quite different for a figure-eight laser, the resulting net MI gain spectra agree quite well, at least in the central region. The frequency range over which positive net MI gain occurs is underestimated by 10% by the CGL model. Both models show vanishing gain at 100 kHz [indicated by the vertical line at $\Omega \sim 0$ in Fig. 3(a)], whereas the frequency with highest gain is near 200 kHz. The Rabi frequency in this case is $\Omega_{\text{Rabi}} = 55$ MHz, and the critical frequency is $\Omega_c = 37$ GHz. They differ by almost three orders of magnitude. Even so, MI occurs for frequencies almost twice as large as Ω_c.

The results for the dye-laser parameters are shown in Fig. 4. Our model predicts that MI occurs in a narrow band near 30 GHz, whereas the CGL model predicts no instability at all! The Rabi frequency Ω_{Rabi} and the critical frequency Ω_c are both close to 24 GHz, which explains why the interaction between the fiber and the two-level system is so highly nonlinear.

Here we find the first meaningful qualitative difference between the full Maxwell–Bloch model and the CGL model. Not surprisingly, the laser power in Fig. 4 is ~60 times the saturation power P_{sat}, which makes the Rabi frequency of the same order as the critical frequency Ω_c.

So for the dye laser of Fig. 4 the interaction between the two-level system on the one side and the GVD and the SPM on the other side cannot be described within a parabolic-gain approximation.

The pump value g_0 at which the cw state loses its stability is often classified as the second threshold,[1] as it announces the onset of unstable behavior. Similarly, we can identify the MI threshold as the gain above which MI occurs. At this threshold, MI occurs only at the frequency corresponding to the peak gain in the MI spectrum, which can be compared with the frequency with which perturbations grow at a Hopf bifurcation. In Figs. 5 and 6 we show the dependence of the MI threshold as a function of θ for the case of the figure-eight laser (Fig. 5) and the dye laser (Fig. 6). The effect of saturable absorption is very dramatic in the case of the figure-eight laser parameters: when θ is larger than $10^{-6} \mathrm{W}^{-1} \mathrm{L}^{-1}$. MI occurs immediately after the first (lasing) threshold. A qualitatively similar dependence is found for the dye laser, where the MI threshold gain decreases from ~ 9 to 1.5 at $\theta = 0.1$. This feature explains why a relatively weak saturable absorber can lead to passive mode locking. Although the presence of a saturable absorber is evidently very useful for the generation of mode-locked pulses, it somewhat obscures our investigation of the interaction between the two-level system and the fiber nonlinearity and dispersion. This explains why for both the figure-eight laser and the dye laser of Figs. 3 and 4, the results hardly change if we consider normal dispersion.

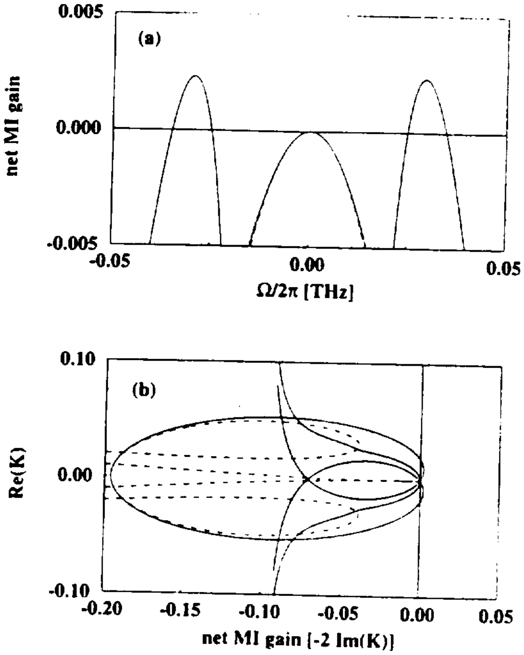

Fig. 4. MI analysis for a dye laser. Similar as in Fig. 3, except for the parameters: $\alpha = 0.1 \mathrm{L}^{-1}$, $g_0 = 3 \mathrm{L}^{-1}$, $\beta_2 = -0.09 \mathrm{ps}^2 \mathrm{L}^{-1}$, $\theta = 0.001 \mathrm{W}^{-1} \mathrm{L}^{-1}$, $\gamma = 0.008 \mathrm{W}^{-1} \mathrm{L}^{-1}$, $T_2 = 2.45$ ps, $T_1 = 10^3$ ps, and $P_{\mathrm{sat}} = 1$ mW.

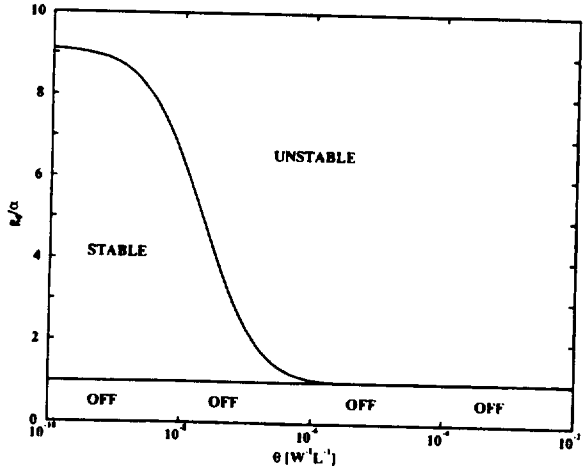

Fig. 5. MI threshold as a function of saturable absorption θ for the fiber laser of Fig. 3.

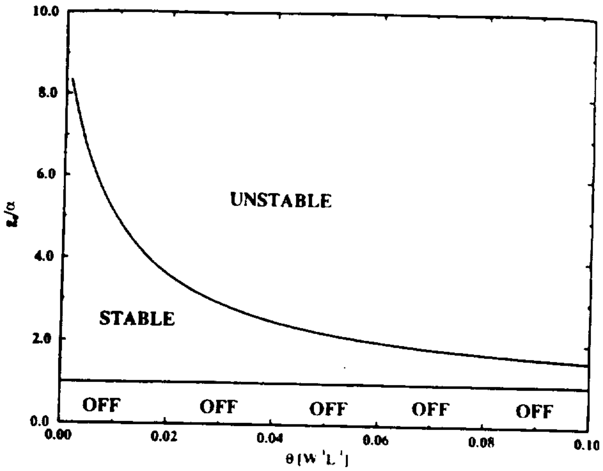

Fig. 6. MI threshold as a function of saturable absorption θ for the dye laser of Fig. 4.

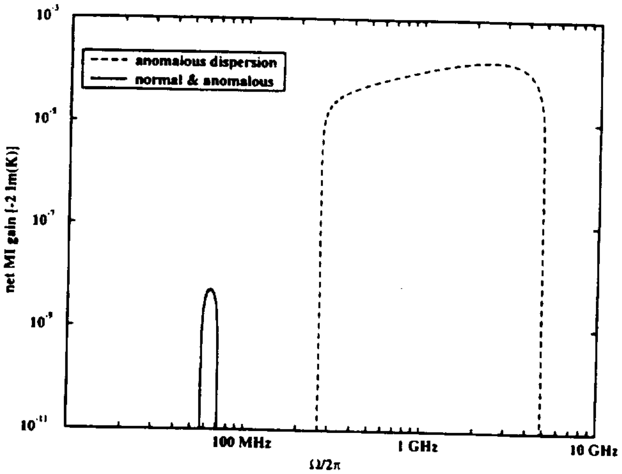

Fig. 7. Comparison of net MI gain spectra in the absence of saturable absorption ($\theta = 0$), for the cases of normal and anomalous dispersion. Other parameters of the fiber laser are the same as in Fig. 3.

We therefore examine the case $\theta = 0$, so that we can consider the sole interaction between the fiber nonlinearity and the two-level system occurring in the absence of saturable absorption. The interesting question is whether atomic coherence can lead to MI in the normal-dispersion regime of the fiber. According to the CGL model, this is not possible.

In Fig. 7 we show, again for a fiber laser, but without saturable absorption (ring-cavity instead of figure-eight

geometry), the net MI gain spectra for $\beta_2 = \pm 0.09\ \mathrm{ps}^2\ L^{-1}$. For anomalous dispersion, we find an approximately 4-GHz-wide MI band centered near 2.5 GHz and a much narrower and much weaker MI band centered near 50 MHz. While the MI band near 2.5 GHz vanishes in the case of normal dispersion, the narrow low-frequency band survives. So, contrary to what the CGL model predicts, the presence of dopants can cause MI instability in the normal-dispersion regime of the fiber. Furthermore, in contrast to the amplifier case (Section 2), any positive value of $-2\,\mathrm{Im}(K)$ should be taken seriously, since, in a laser, even the smallest growth of a perturbation may cause a significant change in the output signal after many round trips in the cavity.

Figure 8 shows the peculiar dependence of this new MI at normal dispersion when the population relaxation time T_1 is decreased from 10 μs to 1.375 μs. Upon decreasing T_1, the new MI band initially grows stronger, while shifting to higher frequencies. Decreasing T_1 further causes the band to weaken and finally to vanish abruptly at ~1.35 μs.

We stress that our results indicate that a fiber ring laser, operating in the normal-dispersion regime, may show unstable behavior at high pump levels, even in absence of additional saturable absorbing mechanisms. At resonance, the strength of the MI in the normal-dispersion regime is rather weak, which would imply that the instability needs to build up during many round trips in the ring laser. In the next section we discuss the effect of detuning on the strength and the nature of this new instability.

5. MODULATION INSTABILITY IN DETUNED FIBER LASERS

With various experimental techniques, e.g., through the use of gratings, one can force a fiber laser to operate away from the gain peak. In our theory this means that we have to deal with the effect of detuning δ. Recall that there is no CGL version for the detuned case, as the group velocity becomes complex in the parabolic-gain approximation. For arbitrary detuning, dispersion relation Eq. (39) reads

$$
\begin{aligned}
&\left[\left(2iK + \frac{g_s}{1+\delta^2} - 4\theta P_0\right)\left(2iK + \frac{g_s}{1+\delta^2}\right)\right.\\
&\quad \left. + \left(\beta_2\Omega^2 - \frac{\delta g_s}{1+\delta^2}\right)\left(\beta_2\Omega^2 + 4\gamma P_0 - \frac{\delta g_s}{1+\delta^2}\right)\right]\\
&\quad \times \{(1 - i\Omega T_2)[(1 - i\Omega T_1)(1 - i\Omega T_2) + I_0]\\
&\quad + \delta^2(1 - i\Omega T_1)\} + \frac{-g_s}{1+\delta^2}\left(2iK + \frac{g_s}{1+\delta^2}\right)\\
&\quad \times \left[(1 - i\Omega T_1)(1 - i\Omega T_2)\right.\\
&\quad \left. - \left(1 - \frac{i\Omega T_2}{1+\delta^2}\right) I_0 + \delta^2(1 - i\Omega T_1)\right]\\
&\quad + \frac{-g_s}{1+\delta^2}\left(2iK + \frac{g_s}{1+\delta^2} - 4\theta P_0\right)\\
&\quad \times \left[(1 - i\Omega T_1)(1 - i\Omega T_2) + \left(1 - \frac{i\Omega T_2\delta^2}{1+\delta^2}\right) I_0\right.\\
&\quad \left. + \delta^2(1 - i\Omega T_1)\right] + \frac{{g_s}^2}{1+\delta^2}\\
&\quad \times [(1+\delta^2)(1 - i\Omega T_1) - I_0]\\
&\quad + 2i\Omega T_2 g_s \frac{\delta^2}{1+\delta^2}\left(2iK + \frac{g_s}{1+\delta^2} - 2\theta P_0\right)\\
&\quad \times \left[1 - i\Omega T_1 - \frac{I_0}{(1+\delta^2)}\right]\\
&\quad + \frac{\delta g_s}{1+\delta^2}\left(\beta_2\Omega^2 - \frac{\delta g_s}{1+\delta^2}\right)\\
&\quad \times [(1+\delta^2)(1 - i\Omega T_1) - I_0]\\
&\quad + \frac{\delta g_s}{1+\delta^2}\left(\beta_2\Omega^2 + 4\gamma P_0 - \frac{\delta g_s}{1+\delta^2}\right)\\
&\quad \times [(1+\delta^2)(1 - i\Omega T_1) + (1 - i\Omega T_2) I_0] = 0, \qquad (41)
\end{aligned}
$$

where $I_0 = P_0/P_{\mathrm{sat}}$. Equation (39) is recovered by putting $\delta = 0$ and $g_s = \alpha - 2\theta P_0$. Equation (41) can be applied as well for amplifiers by treating P_0, g_s, and K as z-dependent quantities.

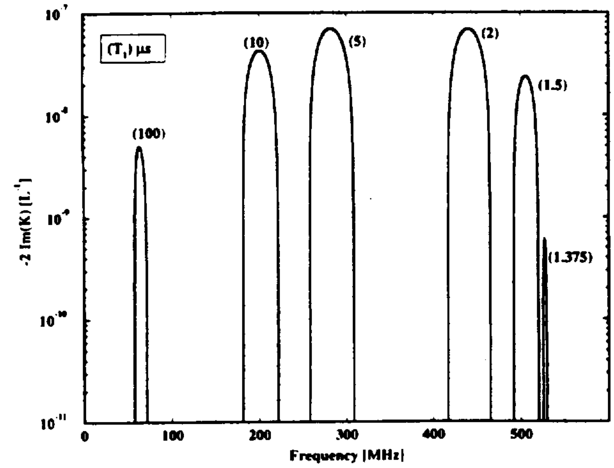

Fig. 8. New MI band at normal dispersion as a function of population relaxation time T_1 (indicated). Other parameters of the fiber laser are the same as those in Fig. 3.

We now use Eq. (41) to investigate the effect of detuning on the MI spectra shown in Fig. 7. The introduction of δ into the problem makes the situation even more complex. Instead of only two frequencies, i.e., the critical frequency Ω_c and the Rabi frequency Ω_{Rabi}, the problem now is governed by the interaction of three frequencies. In Figs. 9 and 10 we show the effect of detuning on the bandwidth and the strength of MI for normal and anomalous dispersion, respectively. Clearly, small detunings have a large effect on the occurrence of MI, and the sign of the detuning also matters. This spectral asymmetry is due to the fiber host nonlinearities. When GVD and SPM are absent, Eq. (41) is symmetric in detuning δ. In the anomalous-dispersion regime (Fig. 10), a small value of the detuning connects the two MI bands, one owing to

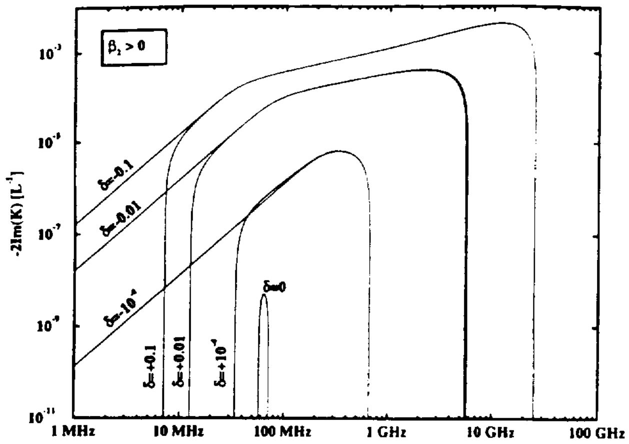

Fig. 9. Effect of detuning on the new MI in the normal-dispersion regime. Parameters identical to those in Fig. 7.

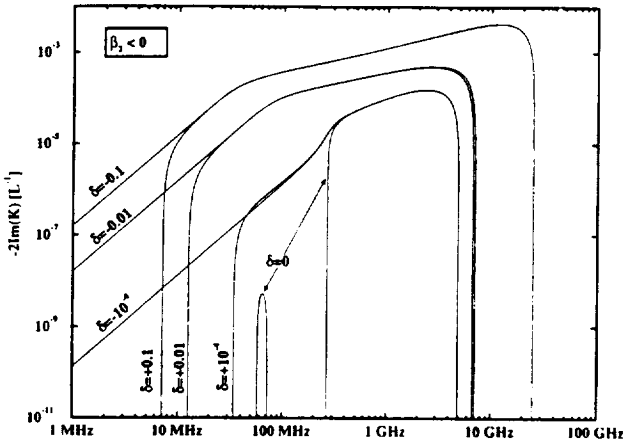

Fig. 10. Similar to Fig. 9, except that the laser now operates in the anomalous-dispersion regime.

the passive fiber MI and the other owing to two-level dynamics. Upon increasing the absolute value of the detuning, the MI bandwidth and the strength increase logarithmically. At large detuning ($\delta = 0.1$), there is no distinction between the normal- and anomalous-dispersion case. For large detuning the instability is apparently dominated by the two-level dynamics.

6. CONCLUSIONS

We have analyzed the occurrence of modulation instability (MI) in fiber lasers and amplifiers by considering the self-phase modulation, group-velocity dispersion, and the saturable host absorption. The gain spectrum has been fully considered, in contrast to the parabolic-gain approximation employed in the complex Ginzburg–Landau (CGL) model. We have derived analytical expressions for the MI dispersion $K(\Omega)$ that naturally reduce to previously reported research for both lasers and amplifiers.

For amplifiers, operating not too heavily saturated and in absence of saturable absorption, no qualitative differences with the CGL description are found, even in regimes where the basic approximations of that model are violated. Quantitatively, however, the differences can be quite substantial. We show that by cooling the fiber amplifier and thereby increasing the dipole dephasing time, the occurrence of MI can be quenched. For heavily saturated amplifiers, we find a new instability located in a narrow frequency band around the Rabi frequency. The CGL model does not predict such an instability. The strength of this new instability is very small, and it is questionable that its effect can be detected in a single-pass amplifier.

In lasers, a different picture emerges, since any growing perturbation may build up over many round trips within the laser cavity. Furthermore, the presence of a weakly saturable absorbing mechanism is shown to greatly enhance the instability. We compare our results with those of Chen *et al.*,[12] who used the CGL model to investigate MI in a dye laser and a figure-eight laser.[12] Our results for the figure-eight laser agree rather well, whereas we find disagreement for the dye laser, which in our model is predicted to have an instability of ~30 GHz. Further indication that the CGL model should be used with caution is given when systems without saturable absorption are studied: for a fiber ring laser operating in the normal-dispersion regime, a narrow MI band of low (~50-MHz) frequencies is found, which is not predicted by the CGL model. This may explain the self-starting of mode-locked Nd-doped fiber lasers.

The effect of detuning on the strength and the bandwidth of the new instability can be substantial, since nonzero detuning effectively introduces a new frequency into the problem. Even for a relatively small detuning, the strength and the bandwidth of MI increase logarithmically, whereas the difference between normal and anomalous dispersion becomes smaller. The fiber nonlinearities cause the MI spectrum to become asymmetric with respect to detuning.

ACKNOWLEDGMENTS

This work was supported in part by the NASA Ames Research Center, the U.S. Army Research Office, and the National Science Foundation under grant PHY94-15583. Helpful discussions with Peter Goorjian are also acknowledged.

REFERENCES

1. C. O. Weiss and R. Vilaseca, *Dynamics of Lasers* (Weinheim, New York, 1991).
2. G. H. M. van Tartwijk and G. P. Agrawal, "Nonlinear dynamics in the generalized Lorenz–Haken model," Opt. Commun. **133**, 565–577 (1997).
3. G. P. Agrawal, "Optical pulse propagation in doped fiber amplifiers," Phys. Rev. A **44**, 7493–7501 (1991).
4. G. P. Agrawal, *Nonlinear Fiber Optics*, 2nd ed. (Academic, New York, 1995).
5. F. Sanchez and G. Stephan, "General analysis of instabilities in erbium-doped fiber lasers," Phys. Rev. E **53**, 2110–2122 (1996).
6. S. Colin, E. Contesse, P. Le Boudec, G. Stephan, and F. Sanchez, "Evidence of a saturable-absorption effect in heavily erbium-doped fibers," Opt. Lett. **21**, 1987–1989 (1996).
7. E. Lacot, F. Stoeckel, and M. Chenevier, "Self pulsing,

chaos and antiphase dynamics in an Er^{3+} doped fiber laser," J. Phys. (France) III **5**, 269–279 (1995).

8. Q. L. Williams and R. Roy, "Fast polarization dynamics of an erbium-doped fiber ring laser," Opt. Lett. **21**, 1478–1480 (1996).
9. S. Bielawski, D. Derozier, and P. Glorieux, "Antiphase dynamics and polarization effects in the Nd-doped fiber laser," Phys. Rev. A **46**, 2811–2822 (1992).
10. H. Zeghlache and A. Boulnois, "Polarization instability in lasers. I. Model and steady states of neodymium-doped fiber lasers," Phys. Rev. A **52**, 4229–4242 (1995); "Polarization instability in lasers: II: Influence of the pump polarization on the dynamics," Phys. Rev. A **52**, 4243–4254 (1995).
11. G. P. Agrawal, "Modulation instability in erbium-doped fiber amplifiers," IEEE Photonics Technol. Lett. **4**, 562–564 (1992).
12. C.-J. Chen, P. K. A. Wai, and C. R. Menyuk, "Self-starting of passively mode-locked lasers with fast saturable absorbers," Opt. Lett. **20**, 350–352 (1995).
13. M. Nakazawa, K. Suzuki, Y. Kimura, and H. Kubota, "Coherent π-pulse propagation with pulse breakup in an erbium-doped fiber waveguide amplifier," Phys. Rev. A **45**, R2682–R2685 (1992).

IEEE JOURNAL OF QUANTUM ELECTRONICS, VOL. 34, NO. 10, OCTOBER 1998

Absolute Instabilities in Lasers with Host-Induced Nonlinearities and Dispersion

Guido H. M. van Tartwijk and Govind P. Agrawal, *Fellow, IEEE*

***Abstract*— We analyze the occurrence of absolute instabilities in lasers that contain a dispersive host material with third-order nonlinearities. Starting from the Maxwell–Bloch equations, we derive general multimode equations to distinguish between convective and absolute instabilities. We find that both self-phase modulation and intensity-dependent absorption can dramatically affect the absolute stability of such lasers. In particular, the self-pulsing threshold (the so-called second laser threshold) can occur at few times the first laser threshold even in good-cavity lasers for which no self-pulsing occurs in the absence of intensity-dependent absorption.**

***Index Terms*— Laser stability, nonlinear optics, optical fiber lasers, optical Kerr effect, optical pulse generation, optical propagation in dispersive media.**

I. INTRODUCTION

ALMOST immediately after the advent of the laser, it was recognized that laser output can become unstable, resulting in irregular power spikes even at a constant pumping level [1]. Over the last 30 years or so, laser instabilities have been studied extensively both from the fundamental and applied viewpoints [2], [3]. The fundamental studies have led to the flourishing field of optical chaos. On the applied side, the development of techniques for controlling chaos are being used to make lasers tailored for specific applications (high power, short pulses, clean far field, etc.).

Since deterministic chaos is studied in a wide variety of disciplines, the understanding of laser instabilities can be improved by referring to plasma and fluid instabilities that have been studied for a long time. A famous example is provided by the Lorenz–Haken equations which are named after the fluid dynamicist Lorenz and the laser theorist Haken [3], [4]. In fluid dynamics, instabilities are categorized into two types: convective and absolute [5]. Convective instabilities are characterized by the growth of localized perturbations upon propagation inside a nonlinear medium, while absolute instabilities exhibit purely temporal dynamics. Absolute laser instabilities have been studied for more than 30 years. The Lorenz–Haken equations describe the dynamics of a homogeneously broadened gain medium in a unidirectional ring-cavity. Although rarely stated explicitly, the Lorenz–Haken equations can only show absolute instabilities. The fundamental concepts such as second laser threshold, self-pulsing, Hopf bifurcation, and different routes to chaos are all formulated within the context of absolute laser instabilities [3].

In the last 15 years or so, new laser systems have been designed that are not easily modeled by the Lorenz–Haken equations. Examples of such lasers are fiber lasers and solid-state (e.g., Ti : sapphire) lasers, which are capable of producing ultrashort optical pulses through passive mode locking while operating at a constant pump power. What these lasers have in common is that the gain is provided by atoms or ions doped inside a host material. As a result, the cavity contains not only a gain element but also other nonlinear elements, which are responsible for nonlinear processes such as self-phase modulation (SPM) and intensity-dependent absorption (IDA) [6]. Also, group-velocity dispersion (GVD) of the host medium plays a nonnegligible role. Because of the dispersive and nonlinear effects, evolution of the optical field over a single round trip must be considered, contrary to the Lorenz–Haken model in which such effects are ignored. This means that the convective nature of any instability must be considered while discussing instabilities for such lasers.

A well-known example of a convective instability occurs in nonlinear fiber optics [6]. Optical fibers, without any gain element and without any longitudinal resonances (no cavity), show a convective instability known as the modulation instability. When the power of a CW optical beam becomes sufficiently large, the combination of SPM and anomalous GVD causes the CW beam to break up spontaneously into a pulse train (and eventually into optical solitons) whose repetition rate depends on the fiber parameters. Mathematically, a linear stability analysis shows that perturbations of the form $\exp[-i(\Omega t - Kz)]$ grow exponentially as $\exp(gz)$ with a growth rate $g = -\mathrm{Im}(K)$ that depends on the frequency of perturbation. The repetition rate of the resulting pulses corresponds to the frequency Ω for which the growth rate g is maximum.

Adding gain to the system, e.g., by doping the fiber with rare-earth ions and pumping it optically, can affect considerably the conditions under which modulation instability arises [7]. The instability, however, remains convective in nature. When such a host material (with or without gain) is put into a cavity, the resulting boundary conditions at the cavity mirrors can change the nature of the instability from convective to absolute. Feedback is a necessary ingredient for absolute instabilities to occur. A well-known example is the Ikeda

---

Manuscript received October 31, 1997; revised June 12, 1998. This work was supported in part by the NASA Ames Research Center and the National Science Foundation under Grant PHY94-15583.

G. H. M. van Tartwijk was with the Institute of Optics and Rochester Theory Center, University of Rochester, Rochester, NY 14627 USA. He is now with Philips Optoelectronics B.V., 5656 AA Eindhoven, The Netherlands.

G. P. Agrawal is with the Institute of Optics and Rochester Theory Center, University of Rochester, Rochester, NY 14627 USA.

Publisher Item Identifier S 0018-9197(98)07176-0.

0018–9197/98$10.00 © 1998 IEEE

instability [8], which arises when a Kerr medium is placed in a unidirectional ring cavity. Even without gain and dispersion, the feedback mechanism provided by the cavity results in an absolute instability.

In this paper, we discuss under what conditions a convective instability becomes absolute in a laser. In Section II, we derive, starting from the Maxwell–Bloch equations, a set of Lorenz–Haken-type multimode equations capable of describing the temporal evolution of a laser whose cavity includes optical elements exhibiting dispersion and nonlinearities. The usefulness of this new set of equations is illustrated in Section III by considering a relatively simple case of a single-mode laser. We discuss the stability of that mode as a function of host nonlinearities.

II. MAXWELL–BLOCH EQUATIONS

For definiteness, we focus on a fiber laser although the analysis can be applied to any solid-state laser with some modifications. Our starting point is a set of Maxwell–Bloch equations describing the propagation of optical fields in an optical fiber, doped with rare-earth ions. We write the optical field $\vec{\mathcal{E}}$ and the dopant-induced polarization $\vec{\mathcal{P}}$ as

$$\vec{\mathcal{E}}(x, y, z, t) = \frac{1}{2}\hat{x}F(x, y)A(z, t)\exp[i(K_0 z - \omega_0 t)] + \text{c.c.} \tag{1}$$

$$\vec{\mathcal{P}}(x, y, z, t) = \frac{1}{2}\hat{x}F(x, y)B(z, t)\exp[i(K_0 z - \omega_0 t)] + \text{c.c.} \tag{2}$$

where $\hat{x}$ is the polarization unit vector of light assumed to be linearly polarized along the x axis, $F(x, y)$ is the transverse profile of the fundamental fiber mode, and K_0 is the wavenumber corresponding to the optical frequency ω_0. We assume that the field-polarization direction is preserved upon propagation. After substituting (1) and (2) in Maxwell's equations, modeling dopants as a homogeneously broadened two-level system, and making use of the slowly varying envelope and rotating-wave approximations, we obtain the following equations for the slowly varying complex amplitudes A and B [6]:

$$\frac{\partial A}{\partial z} + \frac{1}{v_g}\frac{\partial A}{\partial t} = \frac{i}{2}B - \frac{1}{2}\alpha A - \frac{i\beta_2}{2}\frac{\partial^2 A}{\partial t^2} + i\gamma|A|^2 A \tag{3}$$

$$T_2\frac{dB}{dt} = -(1 - i\delta)B - iAg \tag{4}$$

$$T_1\frac{dg}{dt} = g_0 - g + \text{Im}(A^* B)/P_s \tag{5}$$

where g is the gain realized by pumping the dopants, α is the optical loss of the host fiber, T_1 is the population lifetime of the dopants, T_2 is the dipole-dephasing time, v_g is the group velocity, β_2 is the GVD coefficient of the host fiber, the complex parameter γ accounts for the host nonlinearities responsible for SPM and IDA, $\delta = (\omega_0 - \omega_A)T_2$ is the scaled detuning between the optical frequency ω_0 and the atomic resonance frequency ω_A, g_0 is the unsaturated gain, and P_s is the saturation power for the dopants. We have written (3)–(5) in such a way that A has units of $\sqrt{\text{W}}$, B has units of $\sqrt{\text{W}}\cdot\text{m}^{-1}$, and g has units of m^{-1}.

The main assumptions in our model are the use of a homogeneously broadened gain medium and the neglect of the stochastic nature of spontaneous emission. The former is not valid for all dopants but is a reasonable assumption for many types of dopants [6]. The latter can be justified if one is interested only in deterministic instabilities.

There are two distinct origins of the nonlinear effects in (3)–(5). The host nonlinearity $\gamma \equiv \gamma' + i\gamma''$ accounts for SPM and IDA effects induced by the silica fiber. The SPM effects are governed by $\gamma' = n_2\omega_0/cA_{\text{eff}}$, where n_2 is the nonlinear-index coefficient, c is the speed of light in vacuum, and A_{eff} is the effective mode area [6]. The effects of IDA are accounted for by γ''. When $\gamma'' > 0$, the loss in the cavity increases with intensity, modeling processes such as two-photon absorption [6]. In contrast, negative values for γ'' imply a decrease in cavity losses with increasing intensity and model fast saturable absorption. The dopant-induced nonlinear effects are governed by the saturation power $P_s \equiv \hbar^2 cn\epsilon_0 A_{\text{eff}}/(2\mu^2 T_1 T_2)$, where $\hbar$ is Planck's constant divided by 2π, μ is the dipole moment of the atomic transition, and n is the background refractive index.

The Maxwell–Bloch equations, together with the boundary conditions imposed by the laser cavity, provide the most general framework for studying laser instabilities. They are capable of handling both convective and absolute instabilities and can show transitions between them. However, their solutions require a numerical approach. Without host nonlinearities ($\gamma = 0$) and without GVD ($\beta_2 = 0$), the steady-state solutions can be obtained, and their linear stability properties have been studied [9]. However, such an approach is quite cumbersome, and it is not easy to carry out the analysis after the inclusion of host nonlinearities and GVD. If one is interested only in absolute instabilities, an analytic approach can be developed, as discussed in the next section.

III. MULTIMODE LASER EQUATIONS

Rather than solving (3)–(5) numerically, we make use of the fact that any cavity supports a set of longitudinal modes whose field distribution $f_m(z, t)$ reproduces itself after each round trip inside the cavity. These modes can be obtained by solving (3) with $B = 0$ (no gain in the fiber cavity) and using the appropriate boundary conditions at the cavity mirrors. For a high-Q laser cavity, one can distribute the mirror losses throughout the cavity and replace the fiber loss α in (3) with $\alpha_T = \alpha + \alpha_M$, where α_M is the distributed mirror loss. The boundary condition then simply becomes $A(L, t) = A(0, t)$, where L is the cavity length. For a Fabry–Perot cavity with mirror reflectivities R_1 and R_2, α_M is given by

$$\alpha_M = \frac{1}{2L}\ln\left(\frac{1}{R_1 R_2}\right). \tag{6}$$

The approximation that the localized mirror loss can be replaced by a distributed loss only holds for a high-Q laser cavity [2].

When dealing with a unidirectional ring laser without host dispersion and nonlinearities, the form of $f_m(z, t)$ becomes simply $\exp[-i\omega_m(t - z/v_g)]$, where ω_m are the mode frequencies and the loss term has been ignored. In the presence of

GVD and SPM. $f_m(z, t)$ may depend on time in a complicated manner, but the temporal patterns remain invariant from round trip to round trip. However, the amplitude of such "temporal modes" can grow from round trip to round trip if an absolute instability occurs. It is thus important to consider time scales describing short-term and long-term dynamics, distinguished on the basis of the round-trip time $T_r = L/v_g$. The field-propagation equation (3) describes both the long-term and short-term effects. By making the coordinate transformation [10]

$$\tau = t - z/v_g, \qquad T = z/v_g \tag{7}$$

we distinguish between the propagation variable τ describing evolution over a single round trip, and the long-term timescale T measured in units of T_r. The steady-state solutions of (3)–(5) are found by putting the derivative with respect to T equal to zero and applying the boundary conditions at the cavity mirrors.

In general, a laser can operate in several longitudinal modes simultaneously. Thus, the laser field can be written as $A_s(\tau) = \sum_m a_m f_m(\tau)$. If this steady state is perturbed, the expansion coefficients a_m become a function of T. We can study the long-term stability of the steady state by expanding the field A and the polarization B into a set of longitudinal modes

$$A(T, \tau) = \sum_m a_m(T) f_m(\tau) \tag{8}$$

$$B(T, \tau) = \sum_m b_m(T) f_m(\tau). \tag{9}$$

When the set of functions $\{f_m(\tau)\}$ is complete, the modal expansion in (8) and (9) is exact. However, it is hard to prove completeness of $\{f_m(\tau)\}$ under all operating conditions. As a practical matter, the infinite sum in (8) and (9) is always truncated. This is justified since only a finite number of longitudinal modes are excited in a laser at a given pump power.

After expansions (8) and (9) are substituted in the Maxwell–Bloch equations (3) and (4) using the coordinate transformation (7), we multiply the equations for a_m and b_m by $f_q^\star$, and integrate them over one round-trip time T_r. We then obtain

$$\begin{aligned}\frac{1}{v_g}\sum_m \frac{da_m}{dT} G_{mq} &= \frac{i}{2}\sum_m b_m G_{mq} - \frac{1}{2}\alpha_T \sum_m a_m G_{mq} \\ &\quad - \frac{i}{2}\beta_2 \sum_m a_m D_{mq} + i\gamma \sum_{m,n,p} a_m a_n^\star a_p C_{mnpq}\end{aligned} \tag{10}$$

$$\begin{aligned}T_2 \sum_m \frac{db_m}{dT} G_{mq} &= -(1 - i\delta)\sum_m b_m G_{mq} - i\sum_m a_m g_{mq}\end{aligned} \tag{11}$$

where the coefficients G_{mq}, D_{mq}, and C_{mnpq} are defined as

$$G_{mq} = \int_0^{T_r} f_m f_q^\star \, d\tau \tag{12}$$

$$D_{mq} = \int_0^{T_r} \frac{d^2 f_m}{d\tau^2} f_q^\star \, d\tau \tag{13}$$

$$C_{mnpq} = \int_0^{T_r} f_m f_n^\star f_p f_q^\star \, d\tau. \tag{14}$$

The values of these coefficients determine how many modes should be considered, i.e., at what point the infinite sum in (8) and (9) can be truncated.

The complex gain coefficient g_{mq} in (11) is given by

$$g_{mq} = \int_0^{T_r} g(T, \tau) f_m(\tau) f_q^\star(\tau)\, d\tau \tag{15}$$

and should be interpreted as follows. When $m = q$, g_{mq} represents the modal gain for the mode $f_{m=q}$, while for $m \neq q$ g_{mq} represents gain modulation because of mode beating (sometimes referred to as population pulsations). From (5), we readily obtain the rate equation for the coefficients g_{mq}:

$$T_1 \frac{dg_{pq}}{dT} = g_0 G_{pq} - g_{pq} - \frac{i}{2P_s}\sum_{m,n}(a_m^\star b_n - a_n^\star b_m) C_{mnpq}. \tag{16}$$

Note that we have not made any assumptions about the orthogonality of the longitudinal modes. The nonorthogonality of longitudinal modes has attracted considerable attention in recent years [11]–[13]. In general, the more "open" a resonator is (the larger the mirror loss), the less orthogonal the longitudinal modes are. For fiber lasers, longitudinal modes are expected to be nearly orthogonal since mirror losses are often kept to a minimum.

If we assume that the functions $\{f_m\}$ are orthonormal, the coefficients G_{mq} reduce to δ_{mq}. The multimode equations (10), (11), and (16) then transform into the following set of Lorenz–Haken-type equations:

$$\begin{aligned}\frac{1}{v_g}\frac{da_q}{dT} &= \frac{i}{2} b_q - \frac{1}{2}\alpha_T a_q - \frac{i}{2}\beta_2 \sum_m a_m D_{mq} \\ &\quad + i\gamma \sum_{m,n,p} a_m a_n^\star a_p C_{mnpq}\end{aligned} \tag{17}$$

$$T_2 \frac{db_q}{dT} = -(1 - i\delta) b_q - i\sum_m a_m g_{mq} \tag{18}$$

$$\begin{aligned}T_1 \frac{dg_{pq}}{dT} &= g_0 \delta_{pq} - g_{pq} \\ &\quad - \frac{i}{2P_s}\sum_{m,n}(a_m^\star b_n - a_n^\star b_m) C_{mnpq}.\end{aligned} \tag{19}$$

Equations (17)–(19) form a complete set of equations describing the dynamics of various longitudinal modes of the laser. They include the effects of host dispersion and nonlinearity through the terms containing β_2 and γ in (17). What constitutes SPM in a propagation-based description now splits into several different kinds of nonlinearities in the modal description. The triple sum in (10) describes the phenomenon of SPM when $m = n = p = q$, cross-phase modulation for $m = q$ and $n = p$, and four-wave mixing for other combinations of m, n, and p [6].

Equations (17)–(19) constitute the main result of this paper. In principle, they can be used to study the phenomenon of passive mode locking by including a larger and larger

number of longitudinal modes as the mode-locked pulses become shorter. When the mode-locked pulse pattern becomes unstable, the laser may switch to a higher harmonic mode-locked operation [14] or even enter a chaotic regime [15]. Equations (17)–(19) can be used to describe such behavior. When the steady-state pattern $A_s(\tau)$ does not vary too rapidly, one can restrict the analysis to a small number of modes, although such a restriction will exclude passive mode-locking. We illustrate the usefulness of (17)–(19) for this case by using a simple example.

IV. A SIMPLE EXAMPLE

The simplest case, analogous to the single-mode Lorenz–Haken model, is obtained from (17)–(19) by setting $m = n = p = q = 1$. The resulting equations become

$$\frac{1}{v_g}\frac{da_1}{dT} = \frac{i}{2}b_1 - \frac{\alpha_T}{2}a_1 + i\tilde{\gamma}|a_1|^2 a_1 \tag{20}$$

$$T_2\frac{db_1}{dT} = -(1 - i\delta)b_1 - ia_1 g_{11} \tag{21}$$

$$T_1\frac{dg_{11}}{dT} = g_0 - g_{11} + \frac{1}{P_s}\,\mathrm{Im}(a_1^\star b_1) \tag{22}$$

where the SPM coefficient is defined as $\tilde{\gamma} = \gamma C_{1111}$. The effect of GVD on a single longitudinal mode merely involves a frequency shift of magnitude $\omega_D = \beta_2 v_g D_{11}/2$, which has been scaled out of the problem by changing the carrier frequency ω_0 to $\omega_0 + \omega_D$. This is equivalent to resetting the atomic detuning by $\delta = \delta + \omega_D$. We normalize these equations using the standard Lorenz–Haken notation and rewrite them in the following way:

$$\frac{dx}{dt} = -\sigma(x - y) + iqx|x|^2 \tag{23}$$

$$\frac{dy}{dt} = -(1 - i\delta)y + (r - z)x \tag{24}$$

$$\frac{dz}{dt} = -bz + \mathrm{Re}(x^\star y) \tag{25}$$

where the normalized time $t = T/T_2$ is measured in units of T_2. The parameters σ, b, r, and q, and the variables x, y, and z are related to quantities appearing in (3)–(5) as

$$\begin{aligned} \sigma &= \alpha_T v_g T_2/2, \qquad & b &= T_2/T_1, \\ r &= g_0/\alpha_T, \qquad & q &= \tilde{\gamma} P_s T_1 v_g, \end{aligned} \tag{26}$$

$$\begin{aligned} x &= \sqrt{b/P_s}\,a_1, \qquad & y &= (ib_1/\alpha_T)\sqrt{b/P_s}, \\ z &= r - g_{11}/\alpha_T. \end{aligned} \tag{27}$$

These equations are identical to the standard Lorenz–Haken equations [3] except for the last term in (23) that is responsible for SPM and IDA occurring because of the host nonlinearities [3].

We now employ the standard linear stability analysis to investigate the stability properties of (23)–(25). First, we look for CW solutions of the form

$$x_s(t) = X\exp[-i(\Delta\omega_s t + \varphi_s)] \tag{28}$$

$$y_s(t) = Y\exp(-i\Delta\omega_s t) \tag{29}$$

$$z_s(t) = z_s \tag{30}$$

where $P = X^2$ is the (scaled) optical field intensity, Y is the (scaled) polarization amplitude, $\Delta\omega_s$ is the frequency shift with respect to the optical frequency ω_0, and φ_s is the phase lag between electric field and polarization. We stress that all these quantities are referring to the single longitudinal mode under consideration.

After substituting (28)–(30) in the evolution equations (23)–(25) and denoting $q \equiv q' + iq''$, the field intensity $P \equiv X^2$ is a positive real solution of the quartic equation

$$\sum_{n=0}^{4} c_n P^n = 0 \tag{31}$$

where the coefficients are given by

$$c_4 = q''^3/\sigma \tag{32}$$

$$c_3 = [1 + 2(1 + \sigma^{-1})]q''^2 + (q''/\sigma)|q|^2 \tag{33}$$

$$\begin{aligned} c_2 = {} & q''(\sigma + 1)^2/\sigma + 2q''(1 + \sigma^{-1})(\sigma + q'') \\ & - 2b\delta q' q''/\sigma - brq''^2 + b|q|^2 \end{aligned} \tag{34}$$

$$\begin{aligned} c_1 = {} & [1 + (q''/\sigma)](\sigma + 1)^2 + b\delta^2 q''/\sigma \\ & - 2bq''(\sigma + 1)(r - 1) - 2b\delta q' \end{aligned} \tag{35}$$

$$c_0 = b\delta^2 - b(r - 1)(\sigma + 1)^2. \tag{36}$$

For each solution P, the accompanying frequency shift $\Delta\omega_s$, inversion z_s, phase lag φ_s, and polarization Y are determined by the following relations:

$$\tan\varphi_s = \Delta\omega_s + \delta = \frac{\delta - q'P}{\sigma + 1 + q''P} \tag{37}$$

$$z_s = r - \left(1 + \frac{q''P}{\sigma}\right)(1 + \tan^2\varphi_s) \tag{38}$$

$$Y = \frac{bz_s}{P}\cos\varphi_s. \tag{39}$$

The presence of SPM affects the CW characteristics of the laser through the frequency shift $\Delta\omega_s$. At resonance, i.e., $\delta = 0$, the laser operates at the gain peak in the absence of SPM. In the presence of SPM, this CW state will be detuned from the gain peak, thus producing less output power. Thus, the effects of detuning δ and the SPM parameter q' either counteract or re-enforce each other. In Fig. 1 we show how the laser power varies with pump at fixed SPM parameter $q' = 1$ for three different detunings δ. In general, the detuning δ increases the first laser threshold, but for $\delta = 5$ and $r > 4$ the laser output power exceeds that obtained for $\delta = 0$. In Fig. 1, we choose $\sigma = 3$ and $b = 1$, typical values used in the context of the Lorenz–Haken model.

The stability of the CW solutions is investigated by performing a linear stability analysis. After writing the perturbed steady states as

$$x(t) = [X + u(t)]\exp\{-i[\Delta\omega_s t + \varphi_s + \psi_A(t)]\} \tag{40}$$

$$y(t) = [Y + v(t)]\exp\{-i[\Delta\omega_s t + \psi_B(t)]\} \tag{41}$$

$$z(t) = z_s + w(t) \tag{42}$$

linearizing the evolution equations for the perturbations u, v, w, ψ (where ψ is the phase difference $\psi_A - \psi_B$), and assuming a solution of the form $\exp(st)$ for u, v, w, ψ, the characteristic eigenvalue equation for s is found to be a quartic

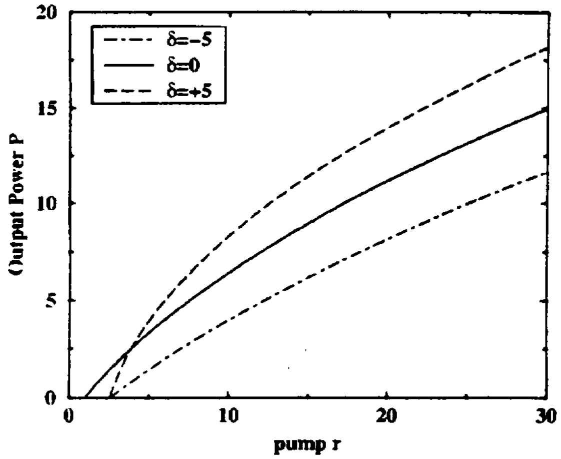

Fig. 1. The laser power P as a function of pump level r in the presence of SPM ($q' = 1$) for three different values of atomic detuning δ (indicated in the figure). Other parameters are $\sigma = 3$ and $b = 1$.

polynomial obtained from the determinant equation as shown in (43), shown at the bottom of the page. When any of the four complex roots of (43) has a positive real part, the steady state under consideration is unstable.

Because of the complexity of the determinant in (43), we do not attempt to find an analytical expression for the second threshold. Instead, we study two cases in detail. One is characterized by the combination $\sigma = 3$ and $b = 1$, and is called the "bad-cavity" laser, while the other ("good-cavity" laser) has the combination $\sigma = b = 1$. The bad-cavity laser has a finite second threshold even in the absence of host nonlinearities, while the good-cavity laser has no second threshold in the Lorenz–Haken limit obtained by setting $q = 0$ [3]. For the resonant case ($\delta = 0$), the second threshold is simply given by $r_{th,2} = \sigma(\sigma + b + 3)/(\sigma - b - 1)$ [3]. A necessary condition, the so-called bad-cavity condition, for the second threshold to exist is $\sigma > b+1$. An analytical expression for the second threshold for arbitrary detuning values was given in [16].

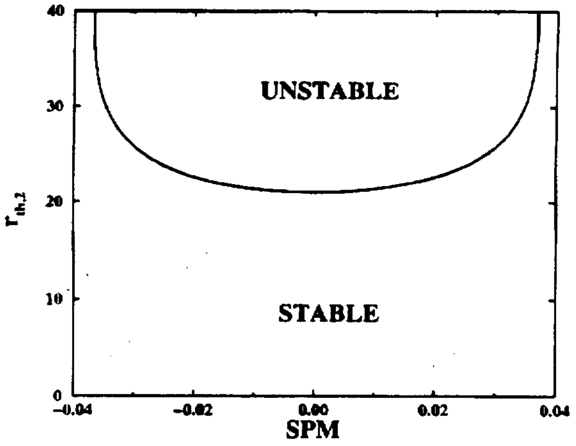

Fig. 2. The effect of SPM on the location of the second threshold at atomic resonance ($\delta = 0$), for the "bad-cavity" laser with $\sigma = 3$ and $b = 1$.

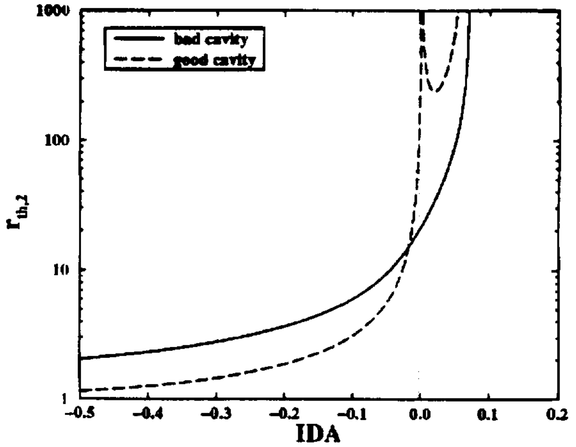

Fig. 3. The effect of IDA on the location of the second threshold at atomic resonance ($\delta = 0$). Solid line: bad-cavity laser with $\sigma = 1$ and $b = 1$. Dashed line: good-cavity laser with $\sigma = 3$ and $b = 1$.

We first consider a laser without IDA and set $q'' = 0$. SPM is then the only host-induced nonlinearity. In Fig. 2, we show the pump parameter at the second threshold as a function of the SPM parameter q' for the bad-cavity laser operating on-resonance ($\delta = 0$). In absence of SPM ($q' = 0$), the second threshold is located at $r = 21$. Quite surprisingly, the global effect of SPM is to stabilize the system: already at $|\gamma'| = 0.04$ the second threshold ceases to exist. This result is surprising since SPM is essential for convective instabilities to occur in passive fibers and fiber amplifiers. From the steady-state analysis above we know that SPM causes a shift in operating frequency away from the gain peak, thus lowering the output power. From a stability point of view this shift can be interpreted as a shift away from the second threshold. The good-cavity laser ($\sigma = b = 1$) shows no second threshold with or without SPM.

Quite a different picture emerges when IDA is included. For both good- and bad-cavity lasers, IDA can reduce the second threshold dramatically, as shown in Fig. 3. In both cases, positive values of q'' account for two-photon absorption while negative values of q'' can be used to describe the effect of a fast saturable absorber. Clearly, fast saturable

$$\begin{vmatrix} s + \sigma + 3q''P & -\sigma \cos \varphi_s & 0 & \sigma Y \sin \varphi_s \\ -(r - z_s) \cos \varphi_s & s + 1 & X \cos \varphi_s & (r - z_s) X \sin \varphi_s \\ -Y \cos \varphi_s & -X \cos \varphi_s & s + b & XY \sin \varphi_s \\ \dfrac{\Delta\omega_s}{X} + 3q'X + (r - z_s) \dfrac{\sin \varphi_s}{Y} & \dfrac{-(\Delta\omega_s + \delta)}{Y} + \dfrac{\sigma \sin \varphi_s}{X} & -\dfrac{X}{Y} \sin \varphi_s & s + \left[\sigma \dfrac{Y}{X} + (r - z_s) \dfrac{X}{Y}\right] \cos \varphi_s \end{vmatrix} = 0 \qquad (43)$$

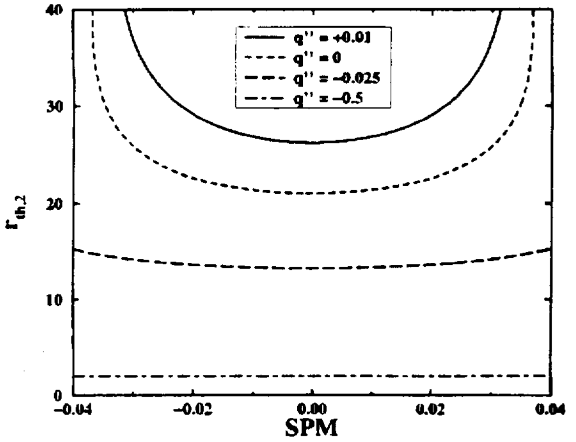

Fig. 4. The location of the second threshold for the bad-cavity laser of Fig. 3, as a function of SPM for four different values of IDA (indicated in the figure).

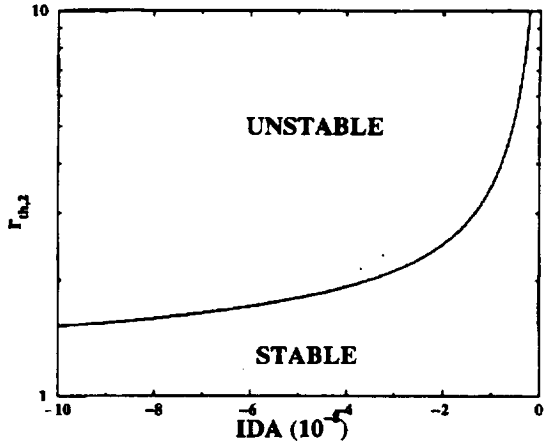

Fig. 5. The location of the second threshold for a fiber ring laser which is forced to oscillate in only one longitudinal mode, as a function of (negative) IDA.

absorption (negative q'') reduces the second laser threshold for both good- and bad-cavity lasers. In the presence of a fast saturable absorber, self-pulsing can therefore occur at pump levels only a few times above the first threshold. We stress that this self-pulsing is not related to passive mode locking because of our assumption of a single longitudinal mode. In fact, the frequency of self-pulsing is related to the relaxation oscillations and is a fraction of the longitudinal-mode spacing.

Fig. 4 shows the combined effect of SPM and IDA for the bad-cavity laser. For four different values of q'', the second laser threshold is shown as a function of the SPM parameter q'. The effects of SPM and negative IDA have opposite effects on the second threshold: SPM stabilizes the laser by increasing the second threshold, while negative IDA destabilizes the laser and reduces the pumping level at which the second threshold occurs. For the good-cavity laser, a qualitatively similar figure is obtained, although in that case no second threshold exists when $q'' = 0$.

Fiber ring lasers usually oscillate in many longitudinal modes simultaneously because their mode spacing (~10 MHz) is a fraction of the gain bandwidth (>1 THz). By using a grating, they can be forced to operate in a single longitudinal mode. When we use typical values for a neodymium-doped fiber laser, $\alpha_T = 46$ km^{-1}, $T_2 = 1.75$ ps, $T_1 = 0.1$ ms, $\gamma = 2.3$ W^{-1}km^{-1}, and $P_s = 11.4$ μW, the dimensionless parameters are $\sigma = 8.84 \times 10^{-6}$, $b = 1.77 \times 10^{-8}$, and $q' = 5.23 \times 10^{-4}$. These values make the single-longitudinal-mode fiber ring laser a good-cavity laser with no second threshold by itself. Fig. 5 shows the effect of fast saturable absorption on the second threshold of such a laser. Even relatively small values of q'' cause a second threshold to exist at quite low pump values. For example, when $q'' = -3.65 \times 10^{-8}$, the second laser threshold exists at a pump level only twice the first laser threshold. This value of q'' corresponds to $\mathrm{Im}(\gamma) = 1.6 \times 10^{-4}$ W^{-1}km^{-1} if we use $C_{1111} = 1$. This is a weak saturable absorption indeed, since it only reduces the losses in the cavity by 0.001% for an intracavity power of 3 W. At the second laser threshold, the relaxation-oscillation frequency is 50 kHz, and self-pulsing will occur with a repetition rate close to that value.

V. CONCLUSIONS

In this paper, we have analyzed the effects of GVD and host nonlinearities (SPM and IDA) on the absolute stability of lasers. Starting from the Maxwell–Bloch equations, we derive a set of multimode laser equations, which govern the absolute dynamics of the laser on a timescale longer than the cavity round-trip time. The presence of a resonator gives rise to longitudinal modes that can differ from their conventional form in the presence of GVD and host-nonlinearities. Our analysis shows the link between the propagation-based (convective) modulation instability and the purely temporal (absolute) instabilities of these spatio-temporal patterns. The latter can occur only in a resonator as absolute instabilities require optical feedback.

To illustrate our formalism, we consider the case of a fiber ring laser forced to oscillate in a single longitudinal mode. The nonlinear dynamics of the slowly varying amplitude of that mode is governed by the Lorenz–Haken equations except that a nonlinear term is added to the field equation. This nonlinear term contains a complex parameter q whose real and imaginary parts account for nonlinear effects such as SPM and IDA, respectively. SPM is found to stabilize the laser, while IDA, in general, destabilizes the laser. Thus, we show that SPM can have a double role as far as stability issues are concerned. On the one hand, it can cause convective instabilities in combination with GVD, which can lead to exponential growth of a localized perturbation. However, once the perturbation fills the entire cavity, its subsequent growth is dictated by the cavity modes. SPM is found to suppress such subsequent growth. IDA induced by fast saturable absorbers, however, quickly gives rise to a second laser threshold at relatively low pump levels. In our single-mode laser, the laser begins to self-pulse at a repetition rate close to the relaxation-oscillation frequency.

ACKNOWLEDGMENT

The authors would like to acknowledge helpful discussions with Dr. P. Goorjian.

REFERENCES

[1] G. Makhov, C. Kikuchi, J. Lambe, and R. W. Terhune, "Maser action in ruby," *Phys. Rev.*, vol. 109, pp. 1399–1400, 1958.

[2] N. B. Abraham, P. Mandel, and L. M. Narducci, "Dynamical instabilities and pulsations in lasers," in *Progress in Optics XXV*, E. Wolf, Ed. Amsterdam, The Netherlands: North-Holland, 1988.

[3] C. O. Weiss and R. Vilaseca, *Dynamics of Lasers*. New York: Weinheim, 1991.

[4] H. Haken, "Analogy between higher instabilities in fluids and lasers," *Phys. Lett.*, vol. 53A, pp. 77–78, 1975.

[5] A. Bers, *Handbook of Plasma Physics*, R. Z. Sagdeev and M. N. Rosenbluth, Eds., *Vol. 1, Basic Plasma Physicsm*, A. A. Galeev and R. N. Sudan, Eds. Amsterdam, The Netherlands: North-Holland, 1983.

[6] G. P. Agrawal, *Nonlinear Fiber Optics*, 2nd ed. New York: Academic, 1995.

[7] G. H. M. van Tartwijk and G. P. Agrawal, "Maxwell–Bloch dynamics and modulation instability in fiber lasers and amplifiers," *J. Opt. Soc. Amer. B*, vol. 14, pp. 2618–2627, 1997.

[8] K. Ikeda, H. Daido, and O. Akimoto, "Optical turbulence: Chaotic behavior of transmitted light from a ring-cavity," *Phys. Rev. Lett.*, vol. 45, pp. 709–712, 1980.

[9] L. A. Lugiato, L. M. Narducci, and M. F. Squicciarini, "Exact linear stability analysis of the plane-wave Maxwell–Bloch equations for a ring laser," *Phys. Rev. A*, vol. 34, pp. 3101–3108, 1986.

[10] H. A. Haus, J. G. Fujimoto, and E. P. Ippen, "Structures for additive pulse mode locking," *J. Opt. Soc. Amer. B*, vol. 8, pp. 2068–2076, 1991.

[11] A. E. Siegman, *Lasers*. Mill Valley, CA: University Science, 1986.

[12] J. Arnaud, "Natural linewidth of anisotropic lasers," *Opt. Quantum Electron.*, vol. 18, pp. 335–343, 1986.

[13] D. Lenstra, "Linewidth modifications due to nonorthogonality, inhomogeneity, and directionality of longitudinal laser modes," *IEEE J. Quantum Electron.*, vol. 29, pp. 954–960, 1993.

[14] S. Arahira, Y. Matsui, and Y. Ogawa, "Mode-locking at very high repetition rates more than terahertz in passively mode-locked distributed-Bragg-reflector laser diodes," *IEEE J. Quantum Electron.*, vol. 32, pp. 1211–1224, 1996.

[15] G. Sucha, S. R. Bolton, S. Weiss, and D. S. Chemla, "Period doubling and quasiperiodicity in additive-pulse mode-locked lasers," *Opt. Lett.*, vol. 20, pp. 1794–1796, 1995.

[16] C. Ning and H. Haken, "Detuned lasers and the complex Lorenz equations: subcritical and supercritical Hopf bifurcations," *Phys. Rev. A*, vol. 41, pp. 3826–3837, 1990.

Guido H. M. van Tartwijk was born in Veghel, The Netherlands, in 1967. He received the M.Sc. degree in theoretical physics from the Eindhoven University of Technology, The Netherlands, in 1990, studying tunneling phenomena in double barrier structures, and the Ph.D. degree from the Vrije Universiteit, Amsterdam, The Netherlands, in 1994. His dissertation was on semiconductor laser dynamics with optical injection and feedback.

In 1995, he worked at the Universitas de les Illes Balears, Palma, Spain, on self-pulsing and broad-area semiconductor lasers. In the same year he was awarded a stipend from The Netherlands Organization for Scientific Research to work one year at the Institute of Optics, Rochester, NY. In 1997, he was a Post-Doctoral Associate at the same institute, working on stability issues of fiber lasers and amplifiers. Presently he is a Research Scientist at Philips Optoelectronics B.V., Eindhoven, The Netherlands.

Govind P. Agrawal (M'83–SM'86–F'96) received the B.S. degree from the University of Lucknow in 1969 and the M.S. and Ph.D. degrees from the Indian Institute of Technology, New Delhi, in 1971 and 1974, respectively.

After holding positions at the Ecole Polytechnique, France, the City University of New York, NY, and AT&T Bell Laboratories, Murray Hill, NJ, in 1989 he joined the faculty of the Institute of Optics at the University of Rochester, Rochester, NY, where he is a Professor of Optics. His research interests focus on quantum electronics, nonlinear optics, and laser physics. In particular, he has contributed significantly to the fields of semiconductor lasers, nonlinear fiber optics, and optical communications. He is an author or co-author of more than 250 research papers, several book chapters and review articles, and three books entitled *Semiconductor Lasers* (New York: Van Nostrand Reinhold, 1993), *Nonlinear Fiber Optics* (New York: Academic, 1995), and *Fiber-Optic Communication Systems* (New York: Wiley, 1997). He has also edited the books *Contemporary Nonlinear Optics* (New York: Academic, 1992) and *Semiconductor Lasers: Past, Present and Future* (Woodbury, NY: AIP Press, 1995).

Dr. Agrawal is a fellow of ~~both~~ the Optical Society of America.